بِسْمِ اللَّهِ الرَّحْمَٰنِ الرَّحِيمِ

كُلُّ نَفْسٍ ذَائِقَةُ الْمَوْتِ ۗ وَإِنَّمَا تُوَفَّوْنَ أُجُورَكُمْ يَوْمَ الْقِيَامَةِ ۖ فَمَن زُحْزِحَ عَنِ النَّارِ وَأُدْخِلَ الْجَنَّةَ فَقَدْ فَازَ ۗ وَمَا الْحَيَاةُ الدُّنْيَا إِلَّا مَتَاعُ الْغُرُورِ

-Surah Ali Imran (185)

Sahih International
Every soul will taste death, and you will only be given your [full] compensation on the Day of Resurrection. So he who is drawn away from the Fire and admitted to Paradise has attained [his desire]. And what is the life of this world except the enjoyment of delusion.

ANALYTICAL MODELING OF EARLY VOLTAGE AND COMMON EMITTER
CURRENT GAIN FOR $Si_{1-y}Ge_y$ HETEROJUNCTION BIPOLAR TRANSISTOR.

by
Fazle Rabbi

A thesis submitted to the Department of Electrical and Electronic Engineering
Bangladesh University of Engineering and Technology
in partial fulfillment of the requirements
for the degree of

MASTER OF SCIENCE IN ELECTRICAL AND ELECTRONIC ENGINEERING

DEPARTMENT OF ELECTRICAL AND ELECTRONIC ENGINEERING
BANGLADESH UNIVERSITY OF ENGINEERING AND TECHNOLOGY,
DHAKA
2012

CERTIFICATION

The thesis titled "ANALYTICAL MODELING OF EARLY VOLTAGE AND COMMON EMITTER CURRENT GAIN FOR $Si_{1-y}Ge_y$ HETEROJUNCTION BIPOLAR TRANSISTOR" submitted by Fazle Rabbi, Roll No.: 100706210P, Session: October 2007 has been accepted as satisfactory in partial fulfillment of the requirements for the degree of MASTER OF SCIENCE IN ELECTRICAL AND ELCTRONIC ENGINEERING on 22nd May 2012.

BOARD OF EXAMINERS

1. _____

   (Md. Ziaur Rahman Khan PhD)   Chairman
   Associate Professor,   (Supervisor)
   Dept of Electrical and Electronic Engineering,
   Bangladesh University of Engineering and Technology,
   Dhaka 1000, Bangladesh.

2. _____

   (Md. Saifur Rahman PhD)   Member
   Professor and Head,   (Ex-officio)
   Dept of Electrical and Electronic Engineering,
   Bangladesh University of Engineering and Technology
   Dhaka 1000, Bangladesh.

3. _____

   (Sharif Mohammad Mominuzzaman PhD)   Member
   Professor,
   Dept of Electrical and Electronic Engineering,
   Bangladesh University of Engineering and Technology
   Dhaka 1000, Bangladesh.

4. _____

   (Md. Anwarul Abedin PhD)   Member
   Professor,   (External)
   Dept of Electrical and Electronic Engineering,
   Dhaka University of Engineering and Technology
   Gazipur, Bangladesh.

DECLARATION

It is hereby declared that this thesis or any part of it has not been submitted elsewhere for the award of any degree or diploma.

Signature of the candidate

_____

(Fazle Rabbi)

TABLE OF CONTENT

LIST OF FIGURES

Name	Title	Page No

LIST OF ABBREVIATION

ABBREVIATION	ELABORATION
BC	Base-collector
BiCMOS	Bipolar -Complementary Metal-Oxide-Semiconductor
BJT	Bipolar Junction Transistor
CB	Conduction Band
CMOS	Confer (compare or consult)
CVD	Chemical Vapour Deposition
DHBT	Double Heterojunction Bipolar Transistor
DOS	Density of States
EB	Emitter-Base
ECL	Emitter Coupled Logic
e.g.	for example
et al.	and co-workers
etc.	et cetera
FET	Field Effect Transistor
GHz	Giga Hertz
HBT	Heterojunction Bipolar Transistor
HEMT	High Elector Mobility Transistor
HFET	Heterojunction Field Effect transistor
IC	Integrated Circuit
i.e.	that is
IGBT	Insulated Gate Bipolar Transistor
IGFET	Insulated Gate Field Effect Transistor
JFET	Junction Field Effect Transistor
MBE	Molecular Beam Epitaxy
MOS	Metal Oxide Semiconductor
MOSFET	Metal Oxide Semiconductor Field Effect Transistor
op-amps	Operational amplifier
RF	Radio Frequency
RFIC	Radio Frequency Integrated Circuit

ABBREVIATION	ELABORATION
SHBT	Single Heterojunction Bipolar Transistor
SoC	System-On-Chip
SOI	Silicon-On-Insulator
VB	Valence Band
VCO	Voltage Controlled Oscillators
vs.	versus

LIST OF TECHNICAL SYMBOLS AND TERMS

SYMBOL	DESCRIPTION
f	Frequency
f_T	Unity gain cutoff frequency
f_{max}	Maximum oscillation frequency
I_B	Base current
I_C	Collector current
I_E	Emitter current
β	Current gain
J_p	Current density for hole
J_n	Current density for electron
J_{nl}	Electron current density for low injection region
J_{nm}	Current density for low injection considering Webster's effect
J_C	Collector current density
γ_E	Emitter charge storage delay time
γ_C	Total delay time from emitter to collector
x	Distance along the base
y	Ge mole fraction
y_C	Ge fraction at the collector end of the base
y_E	Ge fraction at the emitter end of the base
y_{av}	Average Ge mole faction
y_D	Ge dose
a	0.7743
b	$1+3y_{av}$
c	$0.342/[0.342+y_{av}(1-y_{av})]$
v_s	Saturation velocity in Si (107 cm/s)
v_{sA}	Saturation velocity in SiGe alloy
Si	Silicon
Ge	Germanium
SiGe	Silicon Germanium
$D_n(x)$	Diffusion co-efficient of electron

SYMBOL	DESCRIPTION
$D_p(x)$	Diffusion co-efficient of hole
D_{max}	Maximum value of diffusion co-efficient
D_n	Diffusion co-efficient of electron at EB junction
D_{no}	20.72 cm^2/s
$D_{nSiGe}(x)$	Diffusion co-efficient of electron at SiGe alloy
$\mu_n(x)$	Electron mobility
$\mu_p(x)$	Hole mobility
$\mu_{nSiGe}(x)$	Electron mobility inside SiGe alloy
$E(x)$	Electric field
E_C	Critical electric field
$E_{lSiGe}(x)$	Electric field inside SiGe alloy under low injection
$E_{SiGe}(x)$	Electric field inside SiGe alloy under all level of injection
N_{io}	Intrinsic concentration without band gap narrowing
$n_{ie}(x)$	Effective intrinsic carrier concentration
$n_{ieSi}(x)$	Effective intrinsic carrier concentration for Si
$n_{ieSiGe}(x)$	Effective intrinsic carrier concentration for SiGe
$n(x)$	Injected minority carrier for all level of injection
$n_l(x)$	Injected minority carrier for low injection
$n_m(x)$	Electron concentration for low injection considering Webster effect
$\delta n(x)$	Change in injected carrier concentration from high to low injection
$n(0)$	Injected electron concentration at EB junction for all injection
$N_B(x)$	Base doping concentration
$N_B(0)$	Peak base doping concentration
N_r	Reference concentration
$p(x)$	Hole concentration in the base
$p_m(x)$	Hole concentration for low injection considering Webster effect
Q_{Bn}	Stored base charge density for all level of injection
Q_{Bnl}	Stored base charge per unit area for low injection
W_B	Base width
W_{BC}	Width for base collector space charge layer
E_g	Energy gap between conduction and valence band
$D_{EgGe}(x)$	Bandgap narrowing due to the presence of Ge

SYMBOL	DESCRIPTION
$D_{EgHD}(x)$	Bandgap narrowing due to heavy doping
D_{ECG}	Difference between conduction band energies
V_{gGe}	=688 mV
V_{gHD}	=18 mV
V_T	Thermal voltage
V_A	Early voltage
γ	=1~2
γ_1	=0.42
γ_2	=V_{gHD}/V_T=0.69
γ_3	=V_{gGe}/V_T
γ_m	=0.468
γ_r	Ratio of effective DOS in SiGe to the effective DOS in Si
η	Slope of base doping
η_{Ge}	Gradiant of Ge mole fraction
m	Ratio of slope of base doping to base width
m_{Ge}	Ratio of gradient in Ge mole fraction to base width
m_1	=$m\,\gamma_1$
m_2	=$m\,\gamma_2$
m_3	=$m_{Ge}\,\gamma_3$
m_{32}	=m_3-m_2
m_{023}	=m+m_{32}
m_{012}	=$n(1+\gamma_1-\gamma_2)/W_B$
m_{0123}	=m_{012}+m_3
C_{EB}	Emitter base depletion capacitance
C_{BC}	Base collector depletion capcitance
R_B	Intrinsic base resistance
R_C	Collector resistance
r_0	Outpur resistance
g_m	Transconductance
K	Boltzman constant
T	Absolute temperature

SYMBOL	DESCRIPTION
AlGaAs	Aluminium Galium Arsenide
AlGaN	Aluminium Galium Nitride
GaAs	Gallium Arsenide
GaN	Galium Nitride
InAlAs	Indium Aluminium Arsenide
InGaAs	Indiun Galium Arsenide
InP	Indium Phosphide
SiC	Silicon Carbide
q	Electron charge

ACKNOWLEDGEMENTS

ABSTRACT

The Early voltage describes the output conductance and the load drive capability of bipolar transistors, so high Early voltage is desirable for any device. An increase in the collector–base voltage causes a greater reverse bias across the collector–base junction which increases the collector–base depletion region width, and decreasing the channel width of the base, which is defined as "Early effect". The Early effect has been studied extensively in conventional bipolar junction transistors (BJTs). In the present work, closed form analytical model were derived for Early voltage (V_A) and common emitter current gain (β) for uniform, exponential and Gaussian base doping profiles with arbitrary Germanium (Ge) profiles heterojunction bipolar transistor (HBT). Field dependent mobility (D_{nSiGe}), band gap narrowing (BGN) (due to both heavy doping and presence of Germanium content in the base) and electron velocity saturation effects (v_s) were considered in this model. The effects of base doping profiles and Germanium profiles on V_A and β are observed in this work. Here it is observed that if Ge mole fraction at emitter end (y_E) is 0.01 and it increases at collector end (y_C) from 0.01 to 0.3 it increases V_A exponentially. It can be found from this analysis that as y_C increases due to BGN effect, effective intrinsic carrier concentration (n_{ieSiGe}) increases towards base-collector junction which minimizes "Early effect" and increases V_A. For a particular y_C and y_E, V_A found highest for uniform base doping profile and lowest for Gaussian base doping profile. The results show that V_A is proportional with base doping concentration. Also keeping y_C at 0.3 and if y_E vary from 0.01 to 0.3 it reduces V_A. It was also observed that by keeping y_E at 0.01 if y_C can be increased from 0.01 to 0.3 it reduces collector current density (J_{CO}). Effects of Ge mole fraction on D_{nSiGe}, n_{ieSiGe} and electric field (E_{lSiGe}) were studied. Effect of v_s was studied on diffusivity and collector saturation current density (J_{CO}). It is found that v_s has significant impact on both J_{CO} and D_{nSiGe} for uniform and exponential base doping profiles; for Gaussian base doping profile it impact is negligible. Cutoff frequency for HBT calculated in this work. The results obtained by using this analytical model compared with the results available in the previous literature and found in good agreement.

CHAPTER 1

INTRODUCTION

1.1 THE EARLY VOLTAGE AND COMMON EMITTER CURRENT GAIN

The Early effect is the variation in the width of the base in a bipolar junction transistor (BJT) due to a variation in the applied base-to-collector voltage. A greater reverse bias across the collector–base junction increases the collector–base depletion width, decreasing the width of the charge neutral portion of the base. The collector depletion region also increases under reverse bias, comparatively more than the base, because the collector is less heavily doped than the base. The principle governing mechanism in these two widths is charge neutrality. The narrowing of the collector does not have a significant effect as the collector is much longer than the base. The emitter–base junction is unchanged because the emitter–base voltage is the same.
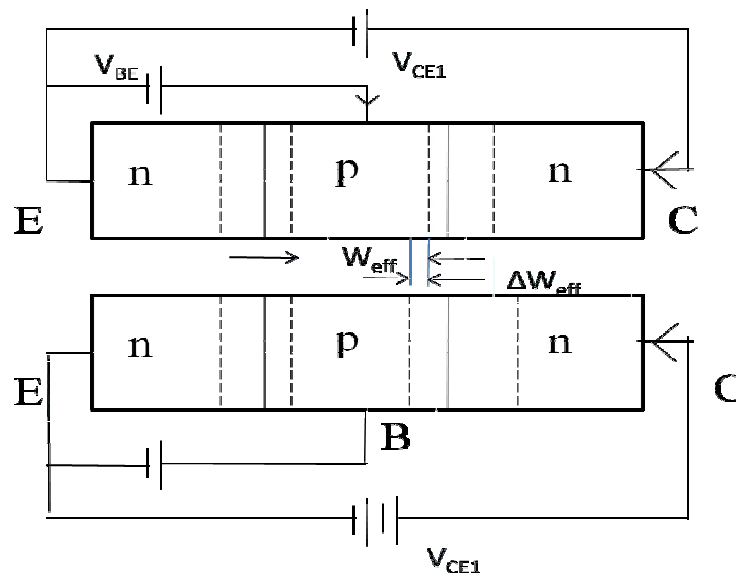
Fig. 1.1: *n-p-n* base width for low collector–base reverses bias (upper picture); narrower *n-p-n* base width for large collector–base reverses bias (lower picture). Hashed areas are depleted regions.
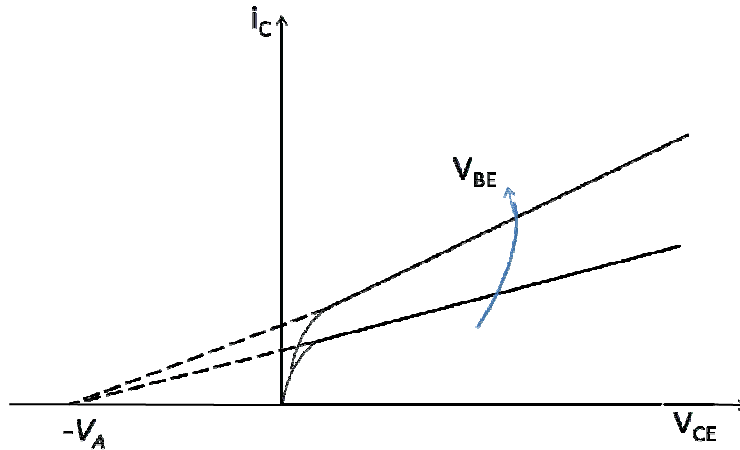
Fig. 1.2. The Early voltage (V_A) as seen in the output-characteristic plot of a BJT.

Base-narrowing has two consequences that affect the current:

- As base width is less than electron depletion length there is a lesser chance for recombination within the "smaller" base region.
- The charge gradient is increased across the base, and consequently, the current of minority carriers injected across the emitter junction increases.

Both these factors increase the collector current of the transistor with an increase in the collector voltage. This increased current is shown in Fig. 1.2. Tangents to the characteristics at large voltages extrapolate backward to intercept the voltage axis at a voltage called the **Early voltage**, often denoted by the symbol V_A.

In the forward active region the Early effect modifies the collector current (I_C) and the forward common-emitter current gain (β_F), as typically described by the following equations [1], [2]

$$I_C = I_S e^{\frac{V_{BE}}{V_T}} \left(1 + \frac{V_{CE}}{V_A}\right)$$

$$\beta_F = \beta_{F0} \left(1 + \frac{V_{CE}}{V_A}\right)$$

Where

- V_{CE} is the collector–emitter voltage
- V_T is the thermal voltage kT/q
- V_A is the Early voltage
- β_{F0} is forward common-emitter current gain at zero bias.

Some models base the collector current correction factor on the collector–base voltage V_{CB} (as described in base-width modulation) instead of the collector–emitter voltage V_{CE} [3]. Using V_{CB} may be more physically plausible, in agreement with the physical origin of the effect, which is a widening of the collector–base depletion layer that depends on V_{CB}.

1.2 THE IMPORTANCE OF EARLY VOLTAGE AND CURRENT GAIN

The Early voltage describes the output conductance and the load drive capability of bipolar transistors so high Early voltage is desirable for any device. The Early effect has been studied extensively in conventional bipolar junction transistors (BJTs). With the advent of advanced material growth techniques like MBE and MOCVD, device structures facilitating high frequency operation. heterojunction bipolar transistors (HBTs) have demonstrated d.c. current gains as high as 112,000 [4] and peak unity gain cut-off frequency (f_T) of more than 175 GHz [5]. HBTs capable of both high frequency and high power performance with f_T of 161 GHz and maximum oscillation frequency (f_{max}) of 167 GHz [6] have also been reported. The performance of experimental HBTs is highly impressive; equally impressive is the lack of theoretical models capable of predicting some of the experimentally observed characteristics of these devices. One of these phenomena is the Early voltage. Effective base width modulation of the transistor due to the applied bias voltage is responsible for Early voltage. In HBTs where the base is heavily doped, the Early effect is expected to be small, resulting in much higher values of Early voltage, as opposed to BJTs. However, as the dimensions of the base region in high-speed HBTs are reduced, the collector current is no longer governed by classical drift-diffusion transport.

1.3 REVIEW OF RECENT WORKS ON EARLY VOLTAGE AND CURRENT GAIN

Several analytical works have been reported on the Early voltage and current gain. Tadao fabricated AlGaAs/GaAs/AlGaAs structure HBT and studied V_A and β for this structure [7]. Tang et al. derived a closed form analytical model of V_A and β for uniform base doping profile HBT with very thin Si emitters [8]. The effect of surface recombination of AlGaAs/GaAs/AlGaAs HBT on the V_A was studied by Chiu et al. [9]. This model did not consider the effect of electric field on mobility while calculating V_A. Effect of Germanium content at the collector base junction on V_A were investigated by Dong et al. [10]. At high doping concentration and high Ge content, neutral base recombination effect on β were analyzed by Ningyue et al. for uniform base doping profile[11]. Prinz et al. studied V_A and β in HBT where bandgap varies across the base [12]. This model is applicable for uniformly doped base and the effect of velocity saturation and field dependent diffusivity were neglected in this model. Yuan et al. modified Prinz's works by including only neutral base re-combination effect on V_A [13]. Early voltage improvement using deep sub-micron technique was proposed by Conrad et al. [14]. Modeling and improvement of current gain for a uniform base doping profile SiC power bipolar junction transistor was done by Domeij [15]. A new bipolar junction transistor for enhanced current gain and reduced hot carrier degradation was proposed by Kumar et al. [16]. High current gain SiC Bipolar Power Transistor were fabricated by Domeij [17]. As velocity saturation and field dependent mobility have strong influence on the parameters of HBT, these effects should consider for calculation V_A and β [18], [19]. Babcock et al. have done a comprehensive investigation of temperature dependence of current gain (β) and Early voltage (V_A) for SiGe-n-p-n transistors [20]. Babcock et al. also done comprehensive investigation of Early voltage (V_A) versus drive current dependence for SiGe-pnp bipolar transistors fabricated on thick-film SOI [21]. Xiao B. et al. generalized SGP model of standard Early voltage for SiGe-n-p-n heterojunction bipolar transistors (HBTs) [22]. Germanium content in the base as well as heavy base doping cause band gap narrowing (BGN) [23]. So BGN due to heavy doping should consider while calculating V_A and β. Zareba derived a new model of V_A considering field dependent diffusivity, velocity saturation and band gap narrowing effects for Gaussian base doping profile HBT [19]. This model did not have a closed form analytical model of the parameter V_A and it was done only for triangular germanium profile in the base. A complete closed form analytical model for V_A

and β for HBT with different base doping profile (uniform, exponential and Gaussian) and trapezoidal/triangular/box germanium profile in the base is yet to be reported where the necessary effects are considered.

1.4 SCOPE OF THIS DISSERTATION

The prime objectives of this research are:

- To derive analytical model for V_A and β for uniform, exponential and Gaussian base doping profile with arbitrary Germanium profiles heterojunction bipolar transistor (HBT). Field dependent mobility, doping dependent mobility, band gap narrowing (BGN) (due to both heavy doping and presence of Germanium content in the base) and velocity saturation effects considered in this model.
- To observe the effects of base doping profile and Germanium profile on V_A and β and to correlate how these two parameters are dependent on diffusion coefficient (D_{nSiGe}), effective intrinsic carrier concentration (n_{ieSiGe}) and electric field (E_{lSiGe}).
- To observe the cut-off frequency of HBT.

Finally the outcome of this research work will be compared with the previous works found in the literature.

1.5 LAYOUT OF THE CHAPTERS

In chapter one previous works on Early voltage and current gain have reviewed and the justification of carrying out the research is given. In chapter two SiGe device physics and basic equations for diffusivity, electric field, collector current density and Early voltage were derived which were used to make close form analytical model for Early voltage and current gain in the next chapters. In chapter three details mathematical analysis were provided to derive closed form of Early voltage and common emitter current gain for three types of base doping profiles and arbitrary Germanium profile. In chapter four graphical representations of Early voltage, current gain, cut-off frequency, intrinsic carrier

concentration, diffusivity were studied with respect to various parameters variation. Also the results obtained by using our models were compared with the results available in the previous research works. Finally this dissertation ends in chapter five containing salient features of this work and possible future field of studies.

CHAPTER 2

BACKGROUND OF WORK

2.1 THE TRANSISTOR

Transistor is one of the greatest achievements in the 20th century and some consider it one of the most important technological breakthroughs in human history. It is the fundamental building block of modern electronic devices and is used in radio, television, telephone, computer and other electronic systems [47]. Transistor is a semiconductor device commonly used to amplify or switch electronic signals. It is made of a solid piece of a semiconductor material, with multiple terminals for connection to an external circuit. Voltage or current applied to one pair of the transistor's terminals changes the current flowing through another pair of terminals.

2.1.1 Brief history of transistor

The first patent for the field-effect transistor principle was documented in Canada by Austrian-Hungarian physicist Julius Edgar Lilienfeld on 22 October 1925. He did not publish any research articles about his devices [48]. German physicist Dr. Oskar Heil in 1934 patented another field-effect transistor. John Bardeen and Walter Brattain On November 1947 at AT&T Bell Labs observed that when electrical contacts were applied to a crystal of germanium, the output power was larger than the input. William Shockley observed the possibility in this invention and as part of a post-war effort to replace vacuum tubes with solid-state devices, worked over the next few months and by December 1947 he greatly succeeded expanding the knowledge of semiconductors. John R. Pierce tailoring the words 'transfer' and 'resistor' and suggested the coined word 'transistor'. According to physicist Robert Arns, legal papers from the Bell Labs patent show that operational versions was built by William Shockley and Gerald Pearson from Lilienfeld's patents.

(a)
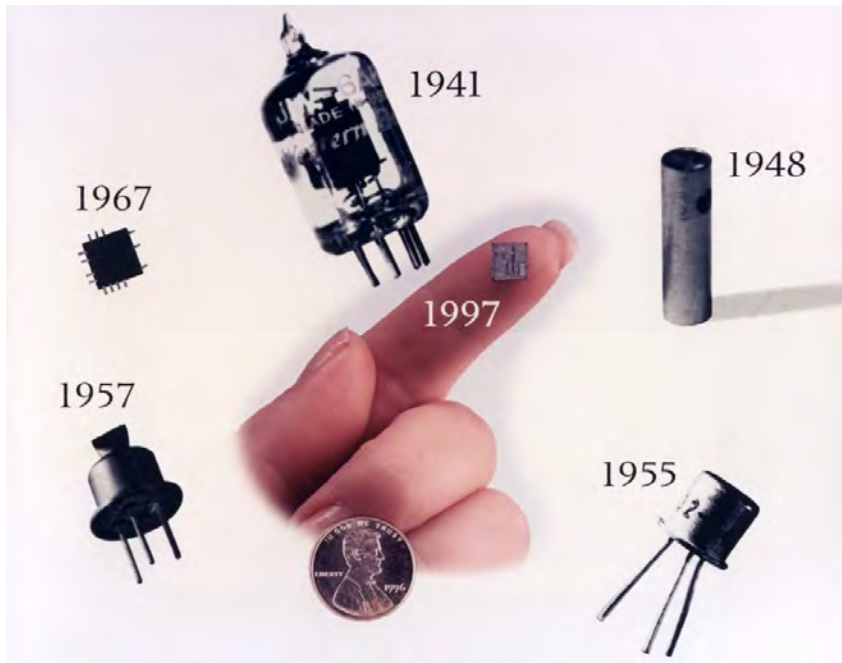
(b)

Fig. 2.1: (a) A replica of the first working transistor (b) Transistor and Integrated Circuits (ICs) chronology [Source: Bell Labs].

They never referenced this work in any of their research papers or historical articles [48].

The first silicon transistor was produced by Texas Instruments in 1954. This was the work of Gordon Teal who had previously worked at Bell Labs, an expert in growing crystals of

high purity. The first MOS transistor actually built at Bell Labs by Kahng and Atalla in 1960 [49].

2.1.2 Category of transistors

Various forms of transistors have been modeled, patented and experimented. A few of them are categorized here in the following table.

Table 2.1 Different type of Transistors (adapted from [50])

Criteria	Subdivision	Category
Structure	Junction Transistor (Bipolar Transistor)	BJT (Bipolar Junction Transistor) HBT (Heterojunction Bipolar Transistor) Insulated Gate Bipolar Transistor (IGBT)
	Field Effect Transistor (Unipolar Transistor)	Junction Field Effect Transistor (JFET) Metal Oxide Semiconductor FET (MOSFET or IGFET)
Polarity		BJT: *npn*, *pnp*
		FET: *n*-channel, *p*-channel
Material		Germanium (Ge), Silicon (Si), Gallium Arsenide (GaAs), Indium Phosphide (InP), Silicon Carbide (SiC) etc.
Power rating		Low, medium, high
Frequency		Radio frequency (RF), microwave etc.
Application		Switch, audio, high voltage, super-beta, matched pair etc.
Packaging		Through hole metal or plastic, surface mount, ball grid array etc.

2.2 THE BIPOLAR TRANSISTOR

As the doping of a semiconductor proceeds, bipolar transistor takes shape. The process of adding controlled impurities into the crystal lattice of a semiconductor is known as doping. The amount of impurity (dopant) added to an intrinsic semiconductor varies its

level of conductivity. Doped semiconductors are often referred to as extrinsic semiconductor. The electrical conductivity of extrinsic semiconductor may be varied not only by the number of impurity atoms but also, by the type of impurity atom and the changes may be thousand folds to million folds. For example- 1 cm^3 of a metal or semiconductor specimen has a number of atoms on the order of 10^{22}. Since every atom in metal donates at least one free electron for conduction in metal, 1 cm^3 of metal contains free electrons on the order of 10^{22}. At the temperature close to 20 °C, 1 cm^3 of intrinsic germanium contains about 4.2×10^{22} atoms , 2.5×10^{13} free electrons and 2.5×10^{13} holes. The addition of 0.001% of arsenic donates an extra 10^{17} free electrons in the same volume and the electrical conductivity increases about 10,000 times [51].

2.2.1 The dopants and doping process of BJT

Intrinsic Silicon (Si) has 4 valence electrons in its outer shell. In Si the most common dopants are group III & group V elements. Group III (boron(B:2,3), aluminum (Al:2,8,3), gallium (Ga:2,8,18,3), indium (In:2,8,18,18,3) and thallium (Tl:2,8,18,32,18,3)) all contain three valence electrons, causing them to function as acceptors when used to dope Si. Group V elements (nitrogen(N:2,5), phosphorus(P:2,8,5), arsenic(As:2,8,18,5), antimony (Sb:2,8,18,18,5) & bismuth(Bi:2,8,18,32,18,5)) have 5 valence electrons, which allow them to act as a donor.

The number of dopant atoms required very small amount to create a difference in the ability of a semiconductor to conduct. When a comparatively small number of dopant atoms are added on the order of one per 100 million atoms, the doping is said to be low or light. When many more dopant atoms are added on the order of one per ten thousand atoms, the doping is referred to as heavy or high. This is often mentioned as n^+ for n-type doping or p^+ for p-type doping. When a semiconductor is doped to such high level, it acts almost like a conductor and is referred as a degenerate semiconductor [51].

Some dopants are added as (usually) the silicon boule is grown using the Bridgeman technique or the Czochralski process, giving each wafer an almost uniform initial doping. For desired device properties, selected areas typically controlled by photolithography are further doped by such processes as diffusion and ion implantation. The latter method being more popular in large production runs because of increased controllability. The molecular beam epitaxy (MBE) or chemical vapor deposition (CVD) technologies are also used in transistor manufacturing where precisely controlled doping is required [52].

2.2.2 Current flow in the n^+-p-n transistor

An n-p-n bipolar junction transistor consists of two back-to-back p-n junctions, who share a thin common region called base. Metal contacts are made to all three regions. The operation of a bipolar junction transistor depends on the forward and the reverse current of the two back-to-back p-n junctions. Base-emitter junction is forward-biased junction, which injects electrons into the center p region and the reversed-biased junction, base-collector junction is reverse biased which collects the injected electrons. Emitter serves as the source of injected electrons and the n region into which electrons are swept by the reverse-biased junction is called the collector. The center region is called the base.

For practical interest, doping concentration of emitter is made very high. Thus it forms an n^+-p-n structure. Fig. 2.2 shows the schematic diagram of an n^+-p-n bipolar junction transistor. To have a good n^+-p-n transistor, it is preferred that almost all the electrons injected by the emitter into the base be collected. To fulfill this requirement neutral base width should be less than the diffusion length of electron in the base. Thus the p-type base region should be narrow. With this requirement satisfied, an average electron injected at the emitter junction will diffuse to the depletion region of the base-collector junction without recombination in the base. A second requirement is that the emitter current (I_E) crossing the emitter junction should be composed almost entirely of electrons injected into the base rather than holes crossing from base to emitter [53].

11
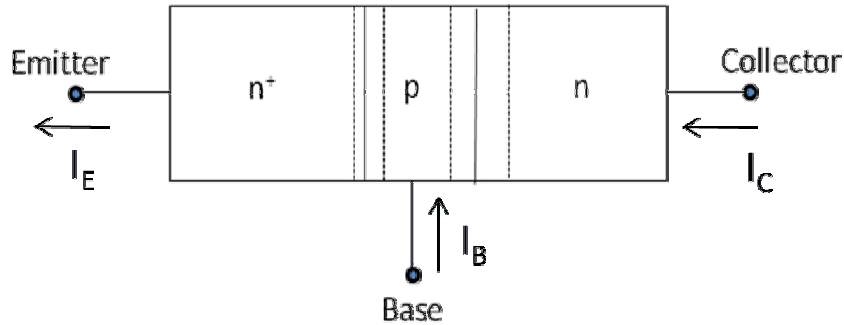
Fig. 2.2: The schematic diagram of an n^+-*p*-*n* bipolar junction transistor. Conventional direction of current flow is assumed.

2.2.3 Advantages of bipolar transistor

The bipolar transistor is still very popular in technology for its high-speed circuits, ultra-high-frequency discreet logic circuits such as emitter coupled logic (ECL), power amplifiers in cellular phones, mixed-signal & precision analog components, microwave power amplifiers and in other applications like fiber-optic communication. The speed advantage (higher frequencies) together with trans-conductance (g_m), high current gain (β) and low $1/f$ noise continue to make the bipolar transistor the device of choice for many demanding applications [54]. One of the important figure of merit of BJTs is the transition frequency f_T, presently which ranges in the GHz level and another important high frequency parameter is the maximum oscillation frequency f_{max} which also ranges in the same level [51].

2.3 HETEROJUNCTION BIPOLAR TRANSISTOR

Two layers or regions of dissimilar crystalline semiconductors interface create heterojunction. It was proposed by W. Shockley in 1948 and patented by him in 1951. These semiconductor materials have unequal band gaps whether a homojunction structure has equal bandgap throughout the region. It is often advantageous to engineer the energy bands in many solid state devices. The *p*-*n* junctions in the Fig. 2.2 are assumed to homojunction (same substrate is used for the emitter, base and collector). If different semiconductors were used as substrates for the emitter, base and collector, then the junctions would be termed as hetero junctions. With two hetero junctions, a bipolar

transistor is identified as double heterojunction bipolar transistor (DHBT) or simply HBT. With one homojunction and another heterojunction, a bipolar transistor is termed as single heterojunction bipolar transistor (SHBT). Typically the emitter of the SHBT is wide bandgap material which allows heavy doping of the base for reduced base resistance while the emitter is more lightly doped reducing the capacitance and improving the high frequency performance. In the DHBT, the collector and emitter have wide bandgap materials allowing the same advantages of the SHBT, with the additional improvement of increased breakdown voltage and decreased minority carrier injection from the base to the collector in saturation mode. heterojunction bipolar transistors are not just an added complication; the use of heterojunctions provides an additional degree of freedom, which can result in vastly improved devices compared to the homojunction counterparts [32].

HBT is actually an improvement of the conventional BJT. Different semiconductor materials in the emitter and base prohibit the injection of electron from the emitter into the base region, since the potential barrier in the valence band is higher than in the conduction band. HBT technology allows a high doping density to be used in the base, reducing the base resistance while maintaining the gain. The idea of employing a heterojunction is as old as the BJT, dating back to a patent from 1951 [47]. Since then many scientists and engineers have contributed to the improvement of HBT and in the year 2000, the Nobel Prize in Physics was awarded with one half jointly to Herbert Kroemer and Zhores Alferov for "developing semiconductor heterostructure used in high-speed and opto-electronics".

In comparison with Si bipolar junction transistors (BJTs), HBTs show better performance in terms of emitter injection efficiency, base-emitter capacitance, base resistance, and cutoff frequency. They also offer good linearity, low phase noise and high power-added efficiency [33].

Table 2.2 Some common materials used for HBT (reproduced from [32])

Material Names	Symbols
Silicon/Silicon Germanium	Si/SiGe
Aluminum Gallium Arsenide/Gallium Arsenide	AlGaAs/GaAs
Indium Phosphide/Indium Gallium Arsenide	InP/InGaAs
Indium Aluminum Arsenide /Indium Gallium Arsenide	InAlAs/InGaAs
Aluminum Gallium Nitride/Gallium Nitride	AlGaN/GaN
Indium Gallium Phosphide/Gallium Arsenide	InGaP/GaAs
Indium Gallium Phosphide/Indium Gallium Arsenide Nitride	InGaP/InGaAsN

Heterojunction structure can be fabricated from different types of elements and compound semiconductor materials. HBTs are named after the materials used in substrate or in the epitaxial layers. Properties of material used determine the characteristics of HBTs and their costs. Table 2.2 shows a list of such common materials used to fabricate HBTs of different genres.

2.3.1 The SiGe device physics

SiGe alloy is introduced into the base of a Si BJT by means of pseudomorphic growth of strained SiGe on Si. This process successfully utilizes bandgap engineering in the Si material system to achieve group III-V like performance while maintaining compatibility with conventional Silicon technology. Introducing Ge into Si improves speed, current gain, noise characteristics and linearity. However, from a physical perspective, the difference in lattice constants between Ge and Si result in SiGe having a slightly higher lattice constant than Si. Ge has smaller bandgap energy than Si (0.66 eV and 1.12 eV respectively); consequently SiGe has a smaller bandgap than Si which facilitates bandgap engineering in Si.

About 75meV reduction in bandgap for every 10% of Ge introduced resulted from the compressive strain in the SiGe film. Since this "band offset" occurs primarily in the valence band, *n-p-n* Si BJTs can be tailored to obtain required performance metrics. The compressive strain also lifts the conduction and valence band degeneracies at the band

extremes. This effectively reduces the density of states (DOS) and improves carrier mobility.
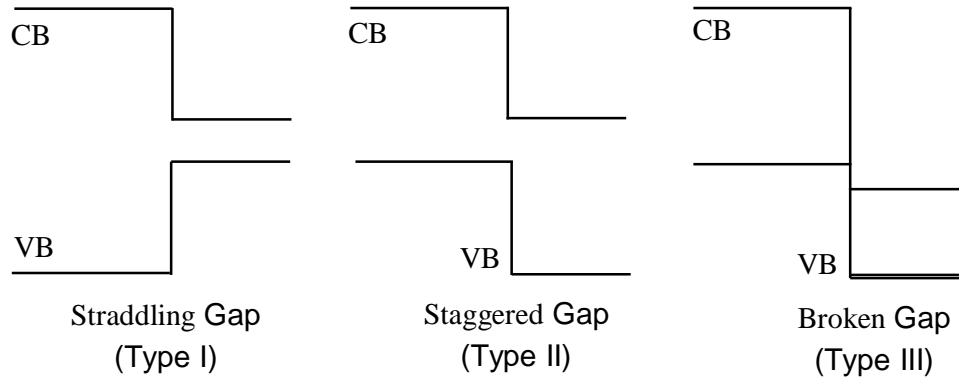
Fig. 2.3: The three types of semiconductor heterojunctions organized by band alignment. Here CB stands for conduction band and VB is the valence band.

Marked performance improvement in both dc and ac characteristics over the Si BJT due to the presence of Si/SiGe heterojunction in the emitter-base (EB) and base-collector (BC) junctions of the HBT. The energy band diagrams of a forward biased graded-base SiGe HBT and a Si BJT are shown in Fig. 2.4.
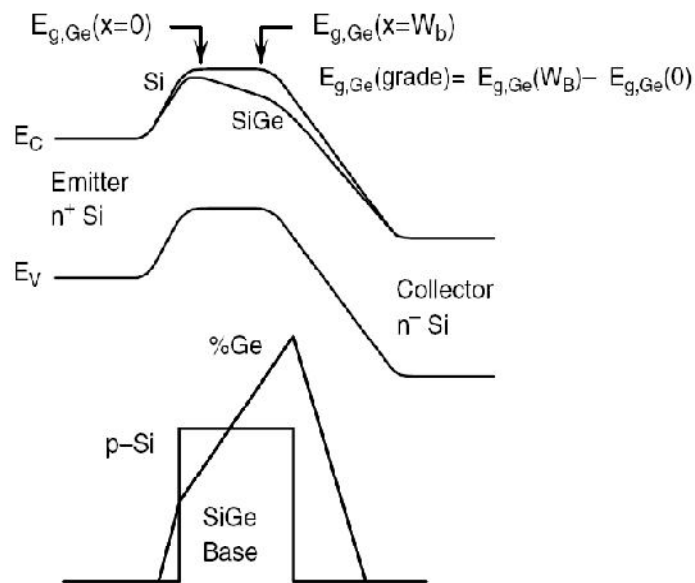
Fig. 2.4: Energy band diagram for a graded base SiGe HBT and a Si BJT, biased in forward active mode at low-injection (reproduced from [34]).

The band structures of graded Ge content in the base are perceptible from the Fig. 2.4. A slight reduction in the base bandgap at the EB junction ($\Delta E_{g,Ge}(x=0)$) and a much larger reduction at the BC junction ($\Delta E_{g,Ge}(x=W_B)$) is observed. This grading of Ge mole fraction across the base induces a built-in quasi-drift field ($((\Delta E_{g,Ge}(x=W_B))-(\Delta E_{g,Ge}(x=0)))/W_B$) in the neutral base region, positively impacting the minority carrier transport. From Fig. 2.4, it is seen that the emitter-base potential barrier is reduced in the SiGe HBT with respect to the Si BJT, thereby allowing increased electron injection from emitter to base. The enhanced electron injection leads to a higher collector current and current gain.
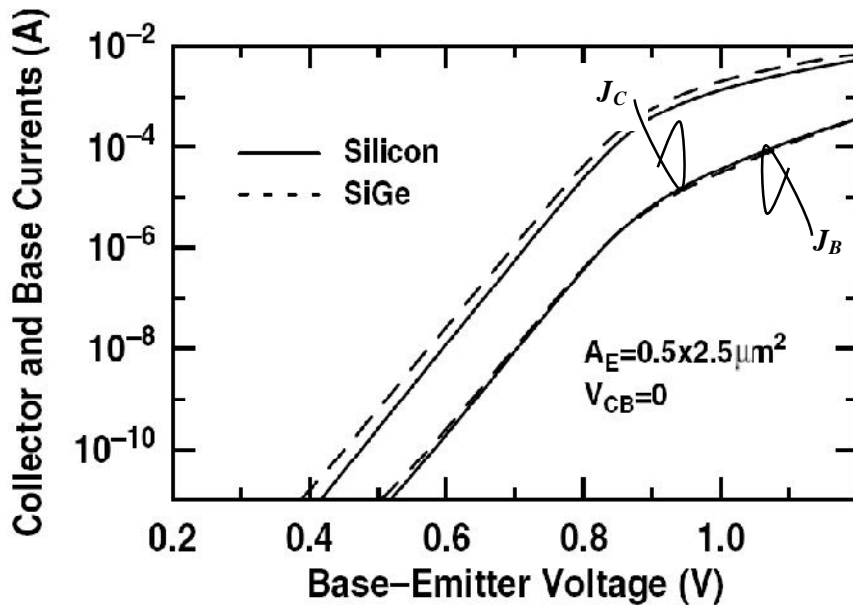
Fig. 2.5: Representative Gummel characteristics for a typical SiGe HBT and a similarly constructed Si BJT (reproduced from [34]).

Fig. 2.5 depicts the Gummel plot for a SiGe HBT as compared to a Si BJT. As expected, the SiGe HBT exhibits higher collector current (J_C) and approximately the same base current (J_B) like the Si BJT. The increase in J_C for the SiGe HBT in turn leads to an increase in current gain (β). The current gain depends linearly on the band offset due to Ge grading across the base and exponentially on the Ge induced band offset at the EB

junction. Therefore, β is dependent on the Ge profile shape and can be modified for particular circuit applications. The introduction of Ge in the base in effect decouples β from the base doping. This fact implies that the base doping can be increased without degrading β. Note that higher base doping reduces the base resistance which has positive implications in terms of frequency response and broadband noise.

Other two important ac features are the transition frequency (f_T) and the maximum oscillation frequency (f_{max}). Ge content in the base has positive impacts on both these parameters. The transition frequency is given by [35]

$$f_T = \frac{1}{2\pi}\left[\tau_E + \tau_B + \frac{W_{BC}}{2v_s} + \left\{\left(C_{EB} + C_{BC}\right)\frac{1}{g_m} + R_C C_{BC}\right\}\right]^{-1} = \frac{1}{2\pi\tau_{EC}} \qquad (1.1)$$

where τ_E is the emitter charge storage delay time, τ_B is the base transit time, W_{BC} is the width of base-collector space-charge layer, v_s is the electron saturation velocity, C_{EB} and C_{BC} are the emitter-base and base-collector depletion capacitances, g_m is the transconductance, R_C is the collector resistance and τ_{EC} is the total delay time from emitter to collector. The grading of Ge across the base induces a built-in electric field in the neutral base region (directed from collector to emitter). This field accelerates the minority carriers across the base which effectively reduces the base transit time. Due to the inverse relationship between the emitter charge storage delay time (τ_E) and current gain (β), the earlier is reduced as the later is higher for the SiGe HBT. Due to the reduction in τ_B and τ_E, f_T of the SiGe HBT increases over that of a Si BJT.

The maximum oscillation frequency of any bipolar transistor is given by [35]

$$f_{max} = \sqrt{\frac{f_T}{8\pi R_B C_{BC}}} \qquad (1.2)$$

where R_B is the ac base resistance which can be reduced by heavy doping in the base region using wide bandgap materials. It is quite evident from equation (1.2) that the maximum oscillation frequency (f_{max}) of the SiGe heterojunction bipolar transistor will

experience a two fold increase once for its higher transition frequency and again for its lower base resistance.

2.3.2 The SiGe HBT

The amount of germanium in the base is graded in SiGe graded heterojunction transistors, making the bandgap narrower at the collector than at the emitter. Field-assisted transport in the base generates by the tapering of the bandgap, which speeds transport through the base and increases frequency response. The SiGe HBTs have better device performance parameters (β, g_m and f_T) compared to silicon BJT. They satisfy the requirements of RF circuits such as modems, mixers, voltage controlled oscillators (VCOs), power amplifiers etc; mixed signal circuits like fractional N synthesizers and analog to digital converters and in the precision analog circuits such as op-amps, band gap references, temperature bias control and current mirrors etc [36]. Further, band gap engineering of SiGe facilitates in reducing forward voltage drop of the emitter-base junction by uniform grading at the emitter-base junction without affecting the other parameters [37] which makes it a best candidate for low voltage applications in wireless phones and other low power battery operated products. In addition to allowing very complex custom designs, high speed and high breakdown voltage SiGe HBTs can be merged with high density CMOS using a mixed signal methodology.
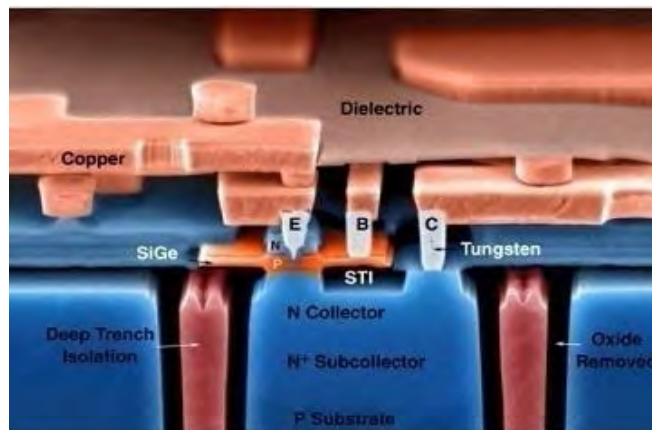
Fig. 2.6: The schematic diagram showing the cross section of a SiGe heterojunction bipolar transistor.(Reproduced from John Cressler's wavepage)

18

The high performance SiGe HBT merge with standard CMOS technology giving rise to a high performance SiGe BiCMOS process without compromising the performance of either the HBT or the CMOS device which is another prime aspect for a SiGe based HBT technology. The combination of SiGe HBTs with scaled BiCMOS to form SiGe HBT BiCMOS technology presents an exciting possibility for system-on-chip (SoC) solution. Further, the use of SiGe devices allows many new functions to be added onto the silicon chip thus potentially reducing cost and power and increasing speed and yield. Ge ion implantation into Si has been successfully demonstrated to form SiGe [38]. But, it is difficult to obtain shallow junctions with sharp impurity profiles in vertical structures. However, recently it has been shown that this technique can be attractive for lateral SoI (Silicon on Insulator) HBT [39].

In SiGe HBT, the introduction of SiGe epitaxial layer into the base of an all-Si bipolar transistor is the main difference from Si BJT. The base region is thus comprised of a Si buffer, boron-doped graded SiGe alloy active layer and a Si cap. Fig. 2.6 depicts the schematic cross-section of a SiGe HBT while Fig. 2.7 portrays Ge profile for a representative first generation SiGe HBT.

The SiGe HBT technology with 50 GHz (1st-generation) [40] and 120 GHz (2nd-generation) [41] peak cutoff frequency are currently in commercial production worldwide from multiple sources and are being deployed in both the commercial and defense sectors. The announcement of a third-generation SiGe HBT technology with 200 GHz peak cutoff frequency [42] and a fourth-generation SiGe HBT technology with over 300 GHz peak cutoff frequency [43], along with the complementary (*n-p-n* & *p-n-p*) SiGe HBTs with peak f_T values above 180 GHz and 80 GHz, respectively [44], have pushed the upper bound on the speeds achievable in these devices considerably higher than previously believed possible, thus vastly increasing the application options for SiGe HBT technology to encompass a wide variety of analog and RF through millimeter-wave systems [45]. While it might be argued that a peak cutoff frequency in excess of 200 GHz is not needed

to support most IC applications, which are currently clustered in the 1-40 GHz range, such extreme levels of performance create a much broader circuit design space where, for instance, a designer has the option to trade frequency response for dramatic reductions in power consumption (10x reduction in bias current in the third-generation devices over second-generation technology for similar operating speeds) [34].
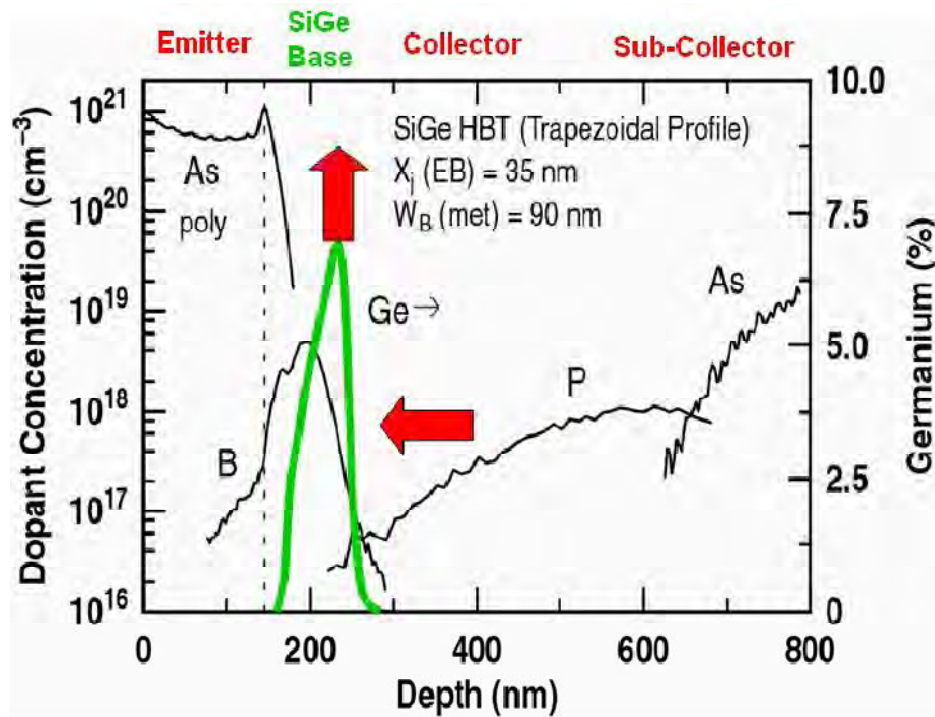
Fig. 2.7: Representative base profiles for a first generation SiGe heterojunction bipolar transistor (reproduced from [34]).

2.3.3 RFIC technology comparison

Gallium arsenide has intrinsically higher low-field electron mobility (6 times higher than Si), transition frequency and breakdown voltage, so it historically been the preferred technology for power amplifiers used in RFIC. The semi-insulating GaAs substrate also helps in developing high-Q passive elements. Due to higher bandgap energies and mobilities, GaAs power amplifiers have higher gain even at lower operating voltage. Even though GaAs has a number of advantages over Si, it also has some disadvantages which need to be considered. The thermal conductivity of GaAs is about 4 times lower than that of Si. This is a particularly difficult challenge for GaAs ICs as the power which

must be dissipated is typically higher than that of Si ICs. Thermal management issue is a major consideration with regards to the ruggedness of the GaAs power amplifiers. Stability and reliability have also been areas of major concern in GaAs technology [46].

SiGe HBT offers a significant challenge to GaAs HBT technology. The unity current gain cutoff frequency of SiGe HBT has reached a level comparable to GaAs technology. SiGe HBT has been demonstrated with f_T beyond 500 GHz [47]. GaAs technology still has a significant performance advantage due to the higher low-field mobility which improves the minimum noise figure, but this is not a major concern in power amplifier design [48]. SiGe technology also cost effective over GaAs due to compatibility with existing Silicon fabrication infrastructure. Finally, a high level of integration can be achieved in SiGe ICs which in turn reduces the packaging complexity.

A summary of the advantages of SiGe technology over other technologies is given below:

- For mobile applications size and power consumption are important considerations. For a given f_T, a SiGe HBT would require only about a third of the collector current as compared to a Si BJT [49]. MOSFETs have lower g_m per mA as compared to BJT/HBT and the current required to obtain the same f_T for MOSFETs is larger [50].
- Breakdown voltages of SiGe HBTs are about twice those of Si BJTs for same f_T. As far as RF CMOS technology is concerned, the breakdown voltage as well as the maximum operating voltage are limited due to thin oxide breakdown and hot-carrier effects [51].
- HBTs have better noise performance since they have higher β and f_T as compared to BJTs. The base resistance of a SiGe HBT is lower than the Si BJT counterpart. CMOS devices have higher minimum noise figure as compared to bipolar devices when biased at the same current density [52].
- By optimizing the Ge profile in the base of a SiGe HBT, much higher Early voltage can be obtained than in BJTs. This results in higher r_o which maximizes gain and also

helps in improving stability. The short-channel RF-MOSFETs have much lower r_o than SiGe HBTs due to increased channel-length modulation effects.

- HBTs have higher current gain than conventional BJTs as a result of which improved linearization by feedback is possible. Cancellation of the base-emitter heterojunction capacitance improves the inter-modulation performance of HBT as compared to MESFET and HEMT. This results in excellent linearity data as reported in [53].

- Due to the advantages of SiGe HBT, such as higher current gain, Early voltage, breakdown voltage and transit frequency, reduced base resistance as well as better transport properties of the base, performance approaching GaAs technologies can be achieved. Moreover, SiGe technology is currently being used to develop electronics for space applications due to their excellent analog and radio frequency performance over an extremely wide range of temperatures [54]. Therefore SiGe technology is a very good choice for high frequency and high temperature electronics at a competitive cost.

2.4 DERIVATION OF MAIN EQUATIONS

In this chapter the main equations were derived which will be used in the next chapters for the derivation of Early voltage and current gain closed form models. These are collector current density, Early voltage and electric field equations. Collector current equation derived from basic equation of drift and diffusion part of current density. Starting from that equation by using boundary conditions for base-emitter and base-collector junction carrier density, collector current equation derived. Early voltage equation also derived from its basic form and using collector current equation. In the same way electric field equation derived. All these equations derived in this chapter used in Chapter 3 by considering various influences to make closed form of Early voltage and common emitter current gain.

2.4.1 Derivation of collector current density (J_{CO}) and common emitter current gain (β)

Here collector current density for SiGe HBT derived by using general transport equation provided by Van Overstraeten [55]. This equation contains two parts, one is diffusion part and another is drift part. Diffusion part is dependent on gradient of electron concentration and drift part is dependent on electric field. Electron concentration at the base-collector junction can be used as boundary condition to solve integral equation [56] [57]. Electron concentration for quasi neutrality of charge within the base region can be found from [58]. Germanium content within the base need to incorporate as Germanium dose for this calculation [59] [60]. Using the boundary conditions in integral equation, J_{CO} as well as β can be obtained.

The electron current density J_n for an arbitrary base doping concentration $N_B(x)$ for SiGe HBT is can be derived from [55]

$$J_n(x) = qD_{nSiGe}(x)\frac{dn_{ieSiGe}(x)}{dx} + q\mu_{nSiGe}(x)n_{ieSiGe}(x)E_{SiGe}(x) \tag{2.1}$$

Where electric field equation is [61]

$$E_{SiGe}(x) = \frac{kT}{q}\left(\frac{1}{p(x)}\frac{dp(x)}{dx} - \frac{1}{n_{ieSiGe}^2(x)}\frac{dn_{ieSiGe}^2(x)}{dx}\right) \tag{2.2}$$

Where q is the charge of electron, D_{nSiGe} is the diffusion coefficient, μ_{nSiGe}, the mobility, n_{ieSiGe}, the effective intrinsic carrier concentration for SiGe HBT.

The boundary condition at the emitter-base junction is [18]

$$n(0) = \frac{n_{ie}^2(0)}{N_B(0)}\exp\left(\frac{qV_{EB}}{kT}\right) \tag{2.3}$$

where V_{EB} is the applied voltage at the emitter-base junction. It is assumed that the electric field at the base-collector junction is large enough to saturate the electron velocity. Then, the electron concentration at the base-collector junction is [56] [57]

$$n(W_B) = \frac{J_n}{qv_s} \tag{2.4}$$

Where v_s is the saturation velocity of electron.

By putting (2.2) in (2.1) and using boundary conditions from (2.3) and (2.4) collector current equation can be found:

$$J_C = J_{CO}e^{(\frac{qV_{BE}}{kT})} = \frac{qe^{(\frac{qV_{BE}}{kT})}}{\int_0^{W_B}\frac{N_B(x)}{n_{ieSiGe}^2(x)D_{nSiGe}(x)}dx + \frac{N_B(W_B)}{n_{ieSiGe}^2(W_B)v_{sA}}} \tag{2.5}$$

Where J_{CO} is collector saturation current density in Silicon Germanium HBT. $N_B(x)$ is the base doping profile, x is the length along base, W_B is the base width and v_{sA} is the saturation velocity within the alloy, V_{BE} is base-emitter voltage, k is the Boltzmann constant and T is the temperature in degrees Kelvin. $N_B(W_B)$ and $n_{ieSiGe}(W_B)$ is doping concentration and effective intrinsic carrier concentration at base-collector junction respectively.

The common emitter current gain (β) can be found from equation (2.5)

$$\beta = \frac{J_{CO}}{J_{BO}} = \frac{q/J_{BO}}{\int_0^{W_B}\frac{N_B(x)}{n_{ieSiGe}^2(x)D_{nSiGe}(x)}dx + \frac{N_B(W_B)}{n_{ieSiGe}^2(W_B)v_{sA}}} \tag{2.6}$$

Where J_{BO} is the base saturation current density.

2.4.2 Early voltage

In this chapter Early voltage derived from it's very basic form. J_{CO} is used in that form to get V_A. To incorporate various factors and for various base doping and germanium profiles this equation will be used in chapter 4.

For a particular V_{BE} from V_A can be found from Fig. 2.8:

$$V_A = \left(J_C\frac{\delta V_{BC}}{\delta J_C}\right)_{V_{BE}=constant} \tag{2.7}$$

(2.7) can be modified as

$$V_A = J_C\left(\frac{\delta W_B}{\delta J_C} \cdot \frac{\delta V_{BC}}{\delta W_B}\right)_{V_{BE}=constant} \tag{2.8}$$
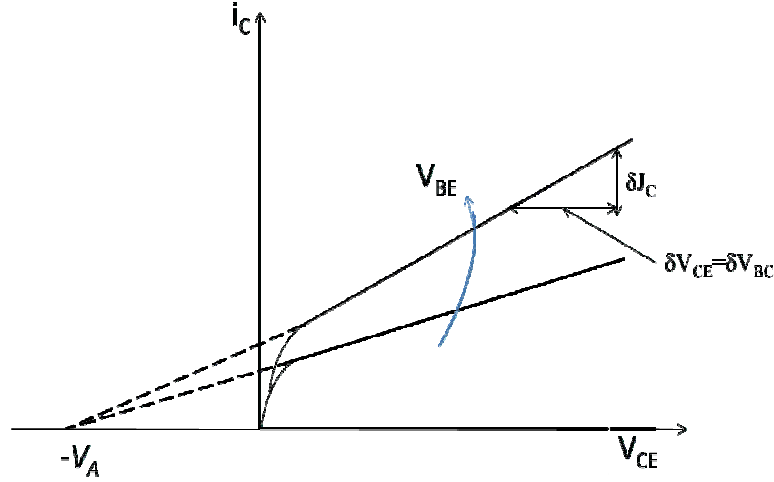
Fig. 2.8 The Early voltage (V_A) as seen in the output-characteristic plot of a BJT.

By solving (2.8) and (2.5) Early voltage equation can be found:

$$V_A = \frac{q n_{ieSiGe}^2 (W_B) D_{nSiGe}(W_B)}{C_{BC}} \times \left(\int_0^{W_B} \frac{N_B(x)}{n_{ieSiGe}^2 (x) D_{nSiGe}(x)} dx + \frac{N_B(W_B)}{n_{ieSiGe}^2 (W_B) v_{sA}} \right)$$

(2.9)

2.4.3 Electric field

Electric field in the base can be written as which is used to make field dependent diffusivity function [62].

$$E(x) = V_T \frac{d}{dx} [ln \, (p(x))] - \frac{1}{q} \frac{d \Delta E_g(x)}{dx}$$

(2.10)

Where,

V_T thermal voltage;

p hole concentration in the base;

$\Delta E_g(x)$ apparent electrical bandgap narrowing in the base, which can be expressed in terms of the effective

$$\Delta E_g(x) = kT ln \left(\frac{n_{ie}^2(x)}{n_i^2} \right)$$

(2.11)

Substituting (2.11) into (2.10) we can get

$$E(x) = V_T \frac{d}{dx} \left[ln \left(\frac{p(x)}{n_{ie}^2(x)} \right) \right]$$

(2.12)

(2.12) can be modified for SiGe doped base as follows:

$$E_{SiGe}(x) = \frac{kT}{q} \left(\frac{1}{p(x)} \frac{dp(x)}{dx} - \frac{1}{n_{ieSiGe}^2(x)} \frac{d n_{ieSiGe}^2(x)}{dx} \right)$$

(2.13)

CHAPTER 3

MATHEMATICAL ANALYSIS

3.1 INTRODUCTION

An accurate analytical model for Early voltage (V_A) and common emitter current gain (β) for $Si_{1-y}Ge_y$ base heterojunction bipolar transistor (HBT) is of great importance for efficient device design. Within the framework of drift and diffusion approaches, an important model should consider the following important effects (a) types of Ge profiles and base doping profiles (b) heavy doping or band gap narrowing effect (c) carrier velocity saturation effect at the collector edge (d) dependence of mobility on electric field and doping concentration. In this chapter closed form analytical models of V_A and β for uniform, exponential and Gaussian base doping profiles for $Si_{1-y}Ge_y$ HBT is derived considering all the above-mentioned effects. Band-gap narrowing (BGN) effect considered to calculate effective intrinsic carrier concentration (n_{ieSiGe}) for both germanium profile and base doping profile. Electron saturation velocity in silicon germanium alloy will differ from silicon material which is considered in diffusivity calculation. The electric filed (E_{lSiGe}) within the base is dependent on the effective intrinsic carrier concentration and hole concentration. To incorporate filed dependency in diffusivity an empirical expression is used. An algebraic equation is used to express trapezoidal/triangular/box germanium profile. V_A and β will be a function of effective intrinsic carrier concentration (n_{ieSiGe}), field dependent diffusion coefficient (D_{nSiGe}) and electric field (E_{lSiGe}). Generalized equations derived for n_{ieSiGe}, D_{nSiGe} and E_{lSiGe} in which only a parameter variation will be required to indicate three (uniform, exponential and Gaussian) types of base doping profiles. These equations of n_{ieSiGe}, D_{nSiGe} and E_{lSiGe} used for a closed form analytical expression of V_A and β.

3.2 DERIVATION OF THE MODEL EQUATIONS

The Ge mole fraction (y) distribution profiles of an n^+-p-n Si$_{1-y}$Ge$_y$-base HBT is shown in Fig. 3.1. For a generalized trapezoidal profile, Ge mole fraction can be expressed as a function of distance along the base

$$y(x) = m_{Ge}x + y_E \tag{3.1}$$

where, x is the distance of a point in the base measured from the emitter-base (EB) junction of the HBT, $m_{Ge} = \eta_{Ge}/W_B$, W_B is the neutral base width, $\eta_{Ge} = y_C - y_E$, y_C and y_E are Ge mole fractions at the collector and emitter end of the base respectively. For $y_E = 0 \neq y_C$, $y_E = y_C$ and $y_E \neq y_C \neq 0$ represents triangular, box and trapezoidal Ge profile respectively [59]. Total Ge content within the base termed as "Ge dose" is calculated as [60]

$$y_D = y_{av}W_B \tag{3.2}$$

where, $$y_{av} = (y_C + y_E)/2 \tag{3.3}$$
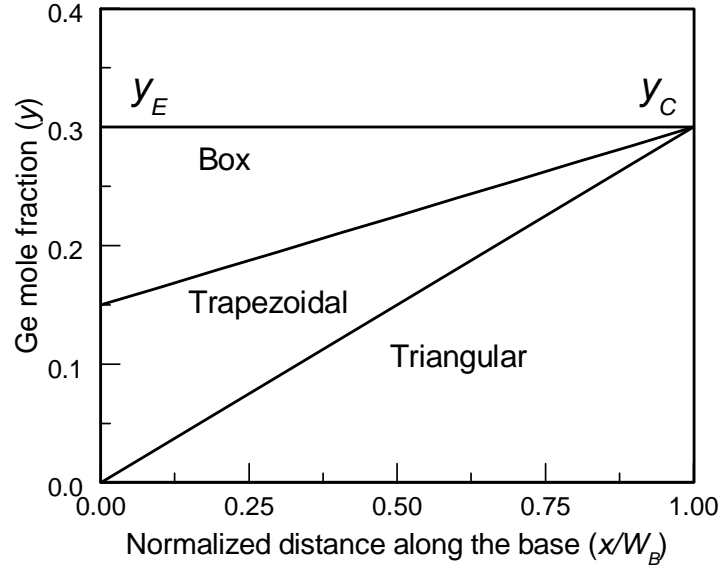
Fig. 3.1: Ge mole fraction distribution within the base of a Si$_{1-y}$Ge$_y$ HBT for various geometric profiles.

The schematic representation of an n^+-p-n transistor is shown in Fig. 3.2. The electron current density J_n and hole current density J_p with arbitrary base doping concentration $N_B(x)$ are given by the transport equations [61],[18],

27

$$- J_n(x) = q \, D_n(x) \frac{dn(x)}{dx} + q \, \mu_n(x) n(x) E(x) \qquad (3.4a)$$

$$J_p(x) = -q \, D_p(x) \frac{dp(x)}{dx} + q \, \mu_p(x) p(x) E(x) \qquad (3.4b)$$

where, $D_n(x)$ & $D_p(x)$ are the diffusion co-efficient (or diffusivity) for electron & hole, $\mu_n(x)$ & $\mu_p(x)$ are the electron & hole mobility, $n(x)$ & $p(x)$ are the electron & hole concentration respectively and $E(x)$ is the electric field at a point x within the base. The direction of J_n in (3.4a) is defined such that it has a positive value. The total current density is the sum of the electron and hole current density.

$$J_c(x) = J_n(x) + J_p(x) \qquad (3.5)$$

The electron diffusion length in silicon is about 500nm even at doping concentration as high as 10^{20} cm^{-3} [62]. As the base width of a modern high-speed HBT is very thin (less than 100nm even 26nm base width is reported in [60]), the carrier recombination in the base region can safely be neglected. So,

$$J_p(x) = 0 \qquad (3.6a)$$

and $$J_c(x) \cong J_n(x) \qquad (3.6b)$$

Therefore, the minority carrier current density J_n within the base becomes constant and is equal to collector current density J_c. In the present work, majority carrier concentration at thermal equilibrium has been neglected.
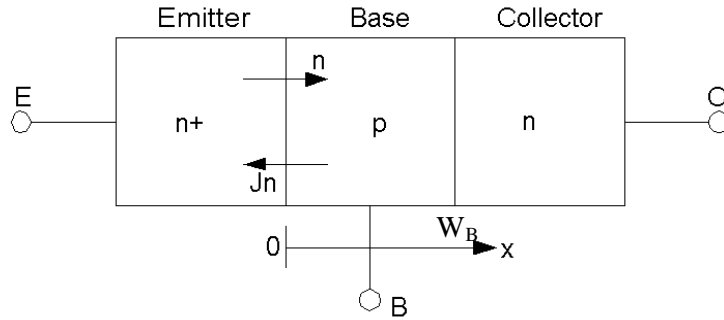
Fig. 3.2: One-dimensional view of an *n-p-n* SiGe heterojunction bipolar transistor showing flow of injected minority carrier and current density.

Electric field considering band gap narrowing effect is [62], [63].

$$E(x) = V_T \frac{d}{dx}\left[\ln\left(\frac{p(x)}{n_{ie}^2(x)}\right)\right] \qquad (3.7a)$$

where, V_T is the thermal voltage and is equal to kT/q, k is the Boltzmann constant, T is the temperature in degrees Kelvin, $n_{ie}(x)$ is the effective intrinsic carrier concentration in the base.

Equation (3.7a) can be written as follows [61]

$$E(x) = V_T \left(\frac{1}{p(x)}\frac{dp(x)}{dx} - \frac{1}{n_{ie}^2(x)}\frac{dn_{ie}^2(x)}{dx}\right) \qquad (3.7b)$$

The first term in (3.7b) represents electric field due to concentration gradient and the second term in (3.7b) represents the quasi-field due to nonuniform band gap narrowing. Carrier mobility and diffusivity are correlated as described by the Einstein's relation [64]

$$D_n(x) = V_T \mu_n(x) \qquad (3.8)$$

The quasi-neutrality of charge within the base of a bipolar transistor is [64]

$$p(x) = n(x) + N_B(x) \qquad (3.9)$$

For low injection, the quasi-neutral condition (3.9) becomes [58]

$$p_l(x) = n_l(x) + N_B(x) \approx N_B(x) \qquad (3.10)$$

Base doping concentration for uniform, exponential and Gaussian base doping profiles are given by (3.11a), (3.11b) and (3.11c) respectively:

$$N_B(x) = N_B(0) \qquad (3.11a)$$

$$N_B(x) = N_B(0)e^{-m_{exp}x} \qquad (3.11b)$$

$$N_B(x) = N_B(0)e^{-m_{gauss}x^2} \qquad (3.11c)$$

$$\text{where} \quad m_{exp} = \frac{\ln(N_B(0)/N_B(W_B))}{W_B} \qquad (3.12a)$$

$$\text{and} \quad m_{gauss} = \frac{\ln((N_B(0)/N_B(W_B))}{W_B^2} \qquad (3.12b)$$

$N_B(0)$ and $N_B(W_B)$ are base doping concentration at the base-emitter junction and base-collector junction respectively.

The low field doping density dependent electron diffusivity in Si, given in [18] can be rearranged as

$$D_{nSi}(x) = D_n \tag{3.13a}$$

$$D_{nSi}(x) = D_n e^{m_{1exp}x} \tag{3.13b}$$

$$D_{nSi}(x) = D_n e^{m_{1gauss}x^2} \tag{3.13c}$$

Equation (3.13a), (3.13b) and (3.13c) represents diffusion coefficient for uniform, exponential and Gaussian base doping profile respectively.

where, $D_n = D_{no} \left(\frac{N_B(0)}{N_r}\right)^{-\gamma_1}$, $D_{no} = 20.72 \frac{cm^2}{s}$, $N_r = 10^{17} cm^{-3}$

$m_{1exp} = m_{exp}\gamma_1$, $m_{1gauss} = m_{gauss}\gamma_1$ and $\gamma_1 = 0.43$.

In the presence of Ge, the electron diffusivity is modified as [65]

$$D_{nSiGe}(x) = b D_{nSi}(x) \tag{3.12b}$$

where, $b=1+3y_{av}$.

The saturation velocity inside the SiGe alloy also differs from that in Si and is [66]

$$v_{sA} = c v_s \tag{3.13}$$

where, $c=0.342/[0.342+y_{av}(1-y_{av})]$ and $v_s=10^7$ cm/s is the saturation velocity in Si.

The empirical expression for field dependent mobility in Si is [67]

$$\mu_{nSi}(|E|,x) = \frac{v_s}{a|E(x)| + E_{cSi}(x)} \tag{3.14a}$$

where, $a=0.7743$. $E_{cSi}(x)$ is the critical electric field and given by

$$E_{cSi}(x) = \frac{v_s}{\mu_{nSi}(x)} \tag{3.14b}$$

The effective intrinsic concentration in SiGe is [65]

$$n_{ieSiGe}^2(x) = \gamma(x) n_{ioSi}^2 \cdot e^{\frac{\Delta E_{geff}(x)}{KT}} \tag{3.15a}$$

where, $n_{ioSi}=1.4 \times 10^{10}$ cm^{-3} is intrinsic carrier concentration in undoped silicon, $\gamma(x)$ is the ratio of the effective density of states in SiGe to the effective density of states in Si as given in [63].

$$\gamma(x) = \exp\left(-\sqrt{5y(x)}\right) \tag{3.15c}$$

Throughout the analysis $\gamma(x)$ considered varying in the base region but only to make close form of V_A and β it is considered fixed [23].

$$\gamma_r = \exp\left(-\sqrt{5y_{av}}\right) \tag{3.15d}$$

$\Delta E_{geff}(x)$ is the effective bandgap narrowing in the SiGe base that can be expressed as

$$\Delta E_{geff}(x) = \Delta E_{gHD}(x) + \Delta E_{gGe}(x) \tag{3.15e}$$

where $\Delta E_{gGe}(x)$ is the bandgap narrowing due to the presence of Ge which is assumed to have a linear dependence on Ge concentration, $\Delta E_{gHD}(x)$ is the bandgap narrowing due to heavy doping effects [23] [68]. An approximation of the Slotboom–de Graaf bandgap narrowing model is used for this term [68].

$$\Delta E_{gHD}(x) = qV_{gHD}\ln\left(\frac{N_B(x)}{N_r}\right) \tag{3.15f}$$

with, $V_{gHD}=18$ mV & the bandgap narrowing due to the presence of Ge is given by [69]

$$\Delta E_{gGe}(x) = qV_{gGe}\,y(x) \tag{3.15g}$$

with, $V_{gGe}=688$ mV. Combining (3.15a)-(3.15g), effective intrinsic concentration in SiGe can be expressed as:

$$n_{ieSiGe}^2(x) = n_{ioSi}^2 e^{\gamma_3 y_e} \left(\frac{N_B(0)}{N_r}\right)^{\gamma_2} e^{(m_3 x - m_2 x^\alpha)}.\gamma(x) \tag{3.15h}$$

where, $\gamma_2=V_{gHD}/V_T=0.69$, $\gamma_3=V_{gGe}/V_T=26.37$, $m_3=\gamma_3.m_{Ge}$,

m_2 for uniform, exponential and Gaussian based doped will be 0, $m_{exp}.\gamma_2$ and $m_{gauss}.\gamma_2$ respectively. α for uniform, exponential and Gaussian base doping profile will be 0,1 and 2 respectively.

3.2.1 Model of Early voltage and current gain

Low injection conditions for a *pn* junction refers to the state where the number of carriers generated are small compared to the background doping density of the material [34].

The subscript '*l*' stands for low injection value of the associated parameter hereafter. From (3.7b) & (3.16), electric field distribution throughout the base of a SiGe HBT becomes:

$$E_{lSiGe}(x) = V_T\left(\frac{1}{N_B(x)}\frac{dN_B(x)}{dx} - \frac{1}{n_{ieSiGe}^2(x)}\frac{dn_{ieSiGe}^2(x)}{dx}\right) \tag{3.16a}$$

Using 3.11(a,b,c), (3.15h) and (3.17a), electric field under low injection will be:

$$E_{lSiGe}(x) = V_T\left(m_3 + 0.31\alpha m x^{(\alpha-1)} - \left(\frac{m_{Ge}\sqrt{5}}{2}\right)\frac{1}{\sqrt{m_{Ge}x + y_E}}\right) \tag{3.16b}$$

Value of m for uniform, exponential and Gaussian base doping profile will be 0, m_{exp} and m_{gauss} respectively and α for uniform, exponential and Gaussian base doping profile will be 0, 1 and 2 respectively.

For arbitrary doped base HBT with arbitrary Germanium profile, the collector current density can be expressed as [70][71].

$$J_C = J_{CO}e^{(\frac{qV_{BE}}{kT})} = \frac{qe^{(\frac{qV_{BE}}{kT})}}{\int_0^{W_B}\frac{N_B(x)}{n_{ieSiGe}^2(x)D_{nSiGe}(x)}dx + \frac{N_B(W_B)}{n_{ieSiGe}^2(W_B)v_{sA}}} \tag{3.17a}$$

J_{CO} is the collector saturation current density in Silicon Germanium HBT. V_{BE} is base-emitter voltage. $N_B(W_B)$ and $n_{ieSiGe}(W_B)$ is doping concentration and effective intrinsic carrier concentration at base-collector junction respectively.

The common emitter current gain (β) can be found from equation (3.17a)

$$\beta = \frac{J_{CO}}{J_{BO}} = \frac{q/J_{BO}}{\int_0^{W_B}\frac{N_B(x)}{n_{ieSiGe}^2(x)D_{nSiGe}(x)}dx + \frac{N_B(W_B)}{n_{ieSiGe}^2(W_B)v_{sA}}} \tag{3.17b}$$

where, J_{BO} is the base saturation current density.

Early voltage is defined as [19]

$$V_A = J_C\left(\frac{\delta W_B}{\delta J_C}\cdot\frac{\delta V_{BC}}{\delta W_B}\right)V_{BE=constant} \tag{3.18a}$$

where V_{BC} is the base to collector voltage.

The Early voltage can be derived by using equation (3.17a) in (3.18a) and is given by

$$V_A = \frac{qn_{ieSiGe}^2(W_B)D_{nSiGe}(W_B)}{C_{BC}} \times \left(\int_0^{W_B}\frac{N_B(x)}{n_{ieSiGe}^2(x)D_{nSiGe}(x)}dx + \frac{N_B(W_B)}{n_{ieSiGe}^2(W_B)v_{sA}}\right) \tag{3.18b}$$

where, C_{BC} is the base-collector junction capacitance.

From equation (3.17b) and (3.18b), product of current gain-Early voltage (βV_A) becomes

$$\beta V_A = \frac{q^2 n_{ieSiGe}^2(W_B) D_{nSiGe}(W_B)}{J_{BO} C_{BC}} \qquad (3.18c)$$

Eq. (3.12b), (3.14a) and (3.16b) is used to calculate $D_{nSiGe}(x)$. By using the value of D_{nSiGe}, n_{ieSiGe}^2 and $E_{lSiGe}(x)$ it can be found β and V_A from (3.17b) and (3.18b) respectively.

By considering ratio of effective density of states in SiGe to that in silicon fixed throughout the base region [23] and then (3.15h) and (3.16b) minimize to (3.19) and (3.20) respectively:

$$n_{ieSiGe}^2(x) = n_{ieSiGe}^2(0) \cdot e^{(m_3 x - m_2 x^\alpha)} \qquad (3.19)$$

Where $n_{ieSiGe}^2(0) = n_{ioSi}^2 e^{\gamma_3 y_e} \left(\frac{N_B(0)}{N_r}\right)^{\gamma_2} \cdot \gamma_r$

$$E_{lSiGe}(x) = V_T(m_3 + 0.31 \alpha m x^{(\alpha-1)}) \qquad (3.20)$$

Using equation (3.19) and (3.20) in (3.18b) V_A for Gaussian base doping profile will be

$$\left(V_A = I_1 + \frac{N_B(W_B)}{n_{ieSiGe}^2(W_B) \cdot v_{sA}} \right) \left(\frac{q n_{ieSiGe}^2(W_B)}{C} \right) \left(\frac{b v_s D_n e^{m_1 W_B^2}}{v_s + a(m_3 + 0.62 m W_B) D_n e^{m_1 W_B^2}} \right) \qquad (3.21)$$

Where

$$I_1 = \frac{a N_B(0) e^{-\frac{m_3^2}{4(m_2 - m_1)}}}{b v_s n_{ieSiGe}^2(0) . 4(m_2 - m)^{3/2}} \left[\sqrt{\Pi} (2m_3(m_2 - m) + 0.62 m m_3) \left\{ erfi\left(\frac{-m_3 + 2(m_2 - m)W_B}{2\sqrt{(m_2 - m)}} \right) - \right. \right.$$

$$erfi\left(\frac{-m_3}{2\sqrt{(m_2 - m)}} \right) \right\} + 1.24 m \sqrt{(m_2 - m)} \left\{ e^{-\frac{(-m_3 + 2(m_2 - m)W_B)^2}{4(m_2 - m)}} - e^{\frac{m_3^2}{4(m_2 - m)}} \right\} \right] +$$

$$\frac{N_B(0) \sqrt{\Pi} e^{-\frac{m_3^2}{4(m_2 - m_1 - m)}}}{2 b D_n n_{ieSiGe}^2(0)(m_2 - m_1 - m)^{1/2}} \left\{ erfi\left(\frac{-m_3 + 2(m_2 - m_1 - m)W_B}{2\sqrt{(m_2 - m_1 - m)}} \right) - erfi\left(\frac{-m_3}{2\sqrt{(m_2 - m_1 - m)}} \right) \right\} \qquad (3.22)$$

β for Gaussian base doping profile is

$$\beta = \frac{J_{CO}}{J_{BO}} = \frac{q/J_{BO}}{I_1 + \frac{N_B(W_B)}{n_{ieSiGe}^2(W_B) v_{sA}}} \qquad (3.23)$$

Where I_1 can be found from (3.22)

V_A for exponential base doping profile will beis

$$V_A = \left(I_2 + \frac{N_B(W_B)}{n_{ieSiGe}^2(W_B).v_{sA}} \right) \left(\frac{q n_{ieSiGe}^2(W_B)}{C} \right) \left(\frac{b v_s D_n e^{m_1 W_B}}{v_s + a m_{032} D_n e^{m_1 W_B}} \right) \tag{3.24}$$

Where $I_2 = \dfrac{N_B(0) a m_{032}}{n_{ieSiGe}^2(0) b v_s m_{132}} \left(1 - e^{-m_{132} W_B} \right) + \dfrac{N_B(0)}{n_{ieSiGe}^2(0) b D_n m_{0132}} \left(1 - e^{-m_{0132} W_B} \right)$

$$\tag{3.25}$$

And $m_{32} = m_3 - m_2$, $m_{032} = m + m_3 - m_2$, $m_{132} = m_1 + m_{32}$, $m_{0132} = m + m_1 + m_{32}.$

β for exponential base doping profile can be found by putting I_2 instead of I_1 in (3.23)

V_A for uniform base doping profile will be is

$$V_A = \left(I_3 + \frac{N_B(0)}{n_{ieSiGe}^2(W_B).v_{sA}} \right) \left(\frac{q n_{ieSiGe}^2(W_B)}{C} \right) \left(\frac{b v_s D_n}{a m_3 D_n + v_s} \right) \tag{3.26}$$

$$\text{where } I_3 = \frac{N_B(0)(a m_3 D_n + v_s)}{n_{ieSiGe}^2(0) b v_s D_n m_3} \left(1 - e^{-m_3 W_B} \right) \tag{3.27}$$

β for uniform base doping profile can be found by putting I_3 instead of I_1 in (3.23).

3.2.2 Cutoff frequency

The cutoff frequency f_T is an important parameter for microwave transistors. It is defined as the frequency at which the common-emitter short-circuit current gain h_{fe} ($=d_{Ic}/d_{Ib}$) is unity [72]. For any transistor having transconductance g_m and a total input capacitance C'_{in}, the small signal output and input currents are given by

$$i_{out} = \frac{dI_{out}}{dV_{in}} v_{in} = g_m v_{in} \tag{3.28}$$

$$i_{in} = v_{in} w C'_{in} \tag{3.29}$$

By equating eq. (3.28) and (3.29), one obtain a general expression of f_T

$$f_T = \frac{g_m}{2\pi C'_{in}} \tag{3.30}$$

In a bipolar transistor, the capacitance component are represented by the sum of

$$C'_{in}=C'_{par}+C'_{dn}+C'_{dp}+C'_{DE}+C'_{DC}+C'_{SC} \tag{3.31}$$

Where,

C'_{par} is parasitic capacitance.

C'_{dn} is diffusion capacitance due to electrons (into base)

C'_{dp} is diffusion capacitance due to holes (into emitter)

C'_{DE} is emitter-base depletion capacitance

C'_{DC} is collector base depletion capacitance

C'_{SC} is space charge capacitance in collector, due to injected electrons

The cutoff frequency can be written as

$$f_T = \frac{1}{2\pi \sum (C'/g_m)} = \frac{1}{2\pi \sum \tau} \tag{3.32}$$

Where τ can be considered as the individual charging time or delay time associated with each capacitance C'/g_m.

$$\frac{C'_{dn}}{g_m} = \left(\frac{qW^2 I_C}{2kTD_n}\right)\frac{1}{g_m} = \frac{W^2}{\eta D_n} \tag{3.33}$$

For uniform base doping profile η is about 2 and for nonuniform base doping profile it is about 7 [73].

Similar diffusion capacitance is due to holes diffusing into the emitter,

$$\frac{C'_{dp}}{g_m} = \frac{N_B W_E W}{2N_E D_n} \tag{3.34}$$

Thus charging time associated with C'_{sc} is

$$\frac{C'_{SC}}{g_m} = \frac{W_{DC}}{2v_s} \tag{3.35}$$

Where, $N_B(0)=10^{19}$ /cm^3, $N_B(W)=7.1\times10^{17}$ /cm^3, $N_E=6\times10^{18}$ /cm^3, $N_C=1.53\times10^{16}$ /cm^3, $WB=20\eta$m, $W_E=20$ ηm, $W_C=40\eta$m, $C'_{DE}=10^{-2}$ F/m^2, $C'_{DC}=2\times10^{-3}$ F/m^2,

An additional delay not related to C/g_m comes from an $R_C C_{DC}$ [74]

The overall cutoff frequency f_T is then given by

$$f_T = \left\{ 2\pi \left[\frac{kT(C'_{par}+C'_{DE}+C'_{DC})}{qI_C} + \frac{W^2}{\eta D_n} + \frac{W_E W}{\theta D_n} + \frac{W_{DC}}{2v_s} + R_C C_{DC} \right] \right\}^{-1} \qquad (3.36)$$

CHAPTER 4

RESULT AND DISCUSSION

4.1 INTRODUCTION

In the previous chapter the mathematical equations related to the analytical modeling of Early voltage and common emitter current gain of $Si_{1-y}Ge_y$ base heterojunction bipolar transistor (HBT) have been derived. These models were used at MATLAB program to get numerical data. Numerical data generated by the program are plotted in this chapter to study the effects of various parameters on V_A and β. The variations of intrinsic carrier concentration, diffusivity, electric field, Early voltage, current gain with respect to various parameters are shown in graphical form separately for three types of base doping profiles and then also shown in the same graph to view the relative variation for three profiles. Then made a discussion on these types of various factors that influence these parameters.

4.2 RESULT AND DISCUSSIONS

The results obtained by using the derivations in the previous chapter are analyzed and discussed below. Base doping concentration $N_B(0)=10^{19}$ cm^{-3} and $N_B(W)=10^{17}$ cm^{-3} considered Gaussian and exponential base doping profile, for uniform base doping profile it was considered 10^{19} cm^{-3}. Collector base junction capacitance $C_{BC}=55\eta F/cm^2$ [12], base width $W_B=30\eta m$ considered for whole analysis.

4.2.1 Distribution of minority carrier within the base (n_{ieSiGe})

Fig. 4.1a through Fig. 4.1d shows effective intrinsic carrier concentration (n_{ieSiGe}) distribution throughout the base region for three types of base doping profile (uniform, exponential and Gaussian) for fixed value of y_E and y_C (y_E is kept 0.01, y_C considered for two values 0.01 and 0.3). From Fig. 1a it is observed that the value of n_{ieSiGe} has no changes for uniform base doping profile in the base region for same value of y_C and y_E

(0.01) but it increases exponentially towards base-collector junction while y_E=0.01 and y_C=0.3. From Fig. 1b it can be observed that, for exponential base doping profile while y_C and y_E has same value (0.01), n_{ieSiGe} gradually decrease towards base-collector junction but it increases for other combination of y_E and y_C (y_E=0.01 and y_C=0.3). The same effect is observed from Fig. 1c for Gaussian base doping profile but the profile of n_{ieSiGe} throughout the base region is not same for exponential and Gaussian base doping profile. A comparative idea can be observed from Fig. 1d for all three types of profile. For small value of y_C (0.01) it is observed that n_{ieSiGe} is greater in base-emitter junction for Gaussian and exponential base doping profile, which decreases gradually towards base-collector junction but for large value of y_C (0.3) the opposite effect is observed. For all three types of profiles n_{ieSiGe} gradually increases from base-emitter junction towards base-collector junction for y_C=0.3. This is due to BGN effect. Increasing y_C decreases band gap which in turn increases probability of carrier concentration in the conduction band. BGN effect occurs mainly two reasons, one for heavy doping and another for Ge content. Heavy doping effect was discussed by Slotboom-de Graaf model [68] and BGN due to Ge content was discussed by Kuo *et. al.* [69]. Effect of Ge-profile on BGN is much higher than base doping concentration. n_{ieSiGe} for HBT with y_C=0.3 is about fifteen times than normal BJT. While both y_C and y_E are small (0.01), n_{ieSiGe} profile is similar to their base doping concentration profiles. Ratio of effective density of states of Si-Ge to silicon ,$\gamma(x)$ also has significant impact on n_{ieSiGe}. It's value changes throughout the base region. Near the base emitter junction it's value is 0.64 and near the base collector junction it reduces to 0.33.
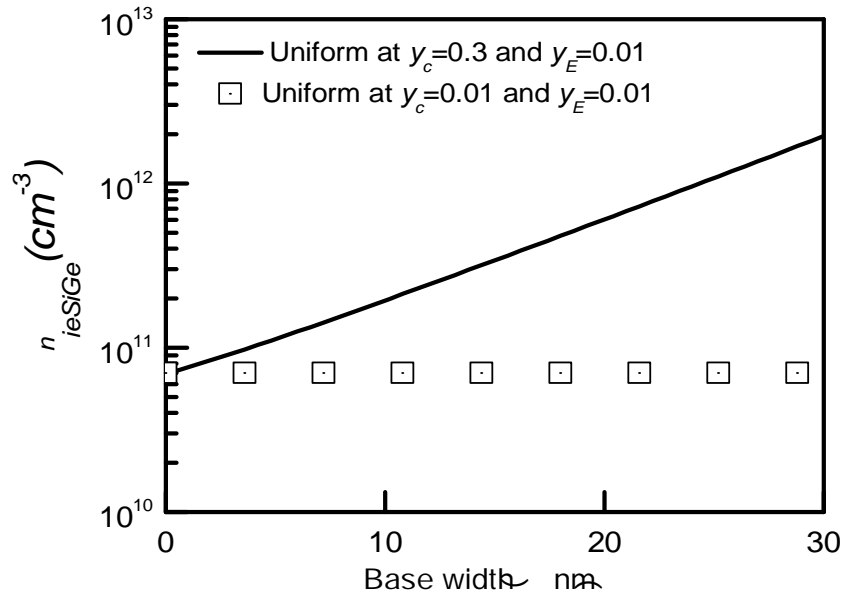
Fig. 4.1a: Effective intrinsic carrier concentration *(n$_{ieSiGe}$)* throughout the base region for uniform base doping profile for two value of y_C (0.01 and 0.3) and single value of y_E (0.01).
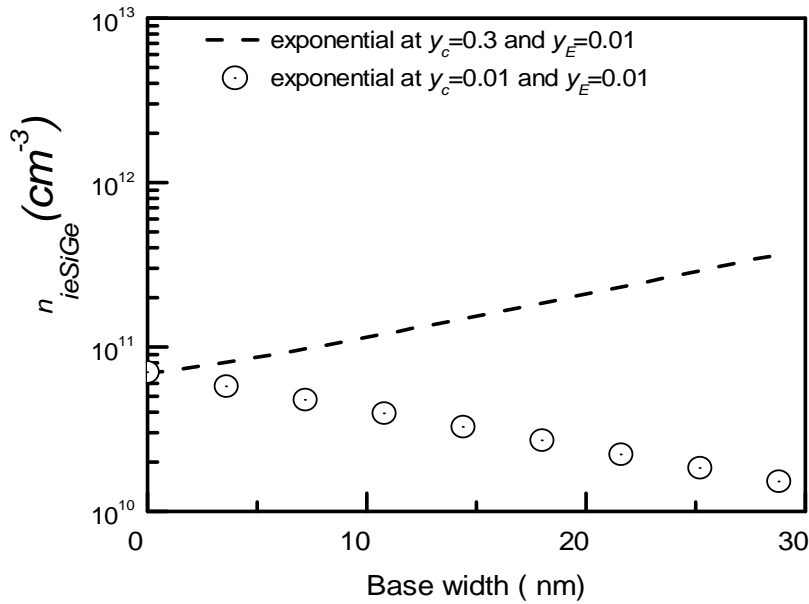
Fig. 4.1b: Effective intrinsic carrier concentration *(n$_{ieSiGe}$)* throughout the base region for exponential base doping profile for two value of y_C (0.01 and 0.3) and single value of y_E (0.01).
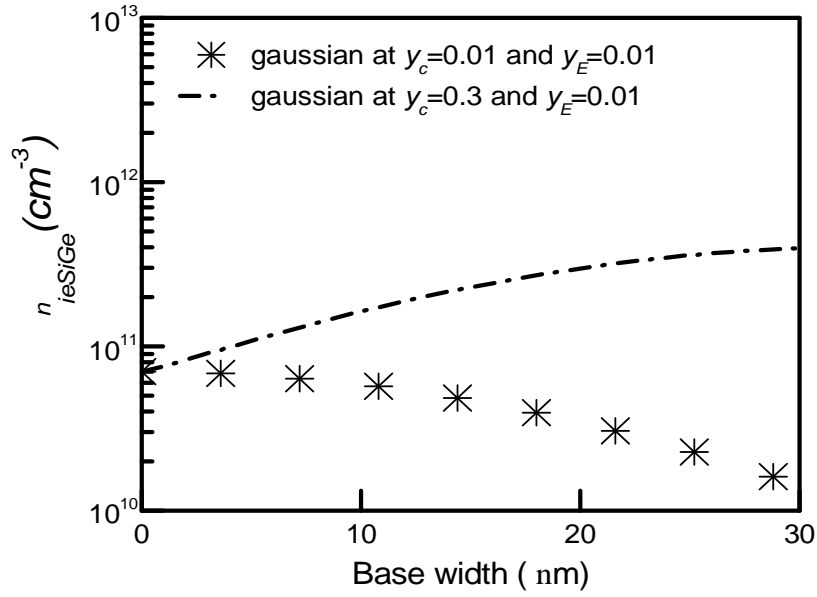
Fig. 4.1c: Effective intrinsic carrier concentration *(n$_{ieSiGe}$)* throughout the base region for Gaussian base doping profile for two value of y_C (0.01 and 0.3) and single value of y_E (0.01).
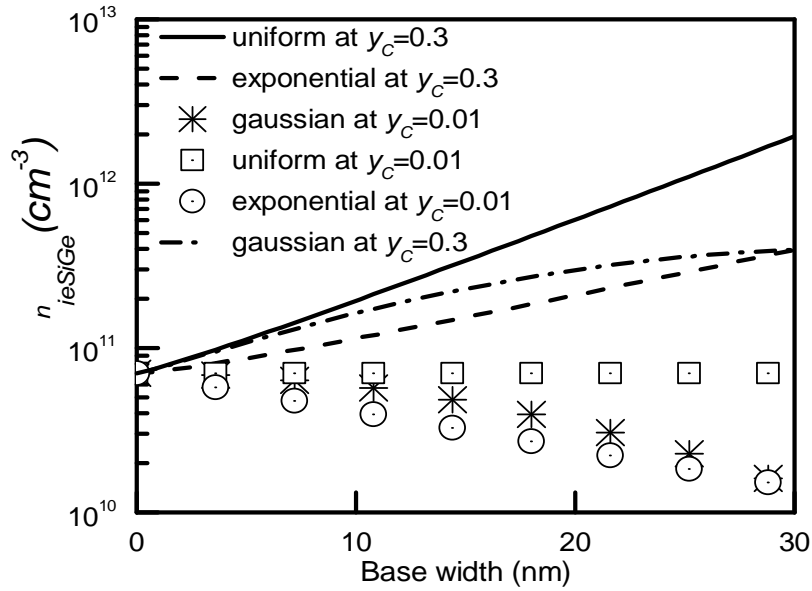

Fig. 4.1d: Effective intrinsic carrier concentration *(n$_{ieSiGe}$)* throughout the base region for three types of base doping profiles for two value of y_C (0.01 and 0.3) and single value of y_E (0.01).

Fig. 4.2a to Fig. 4.2d shows effective intrinsic carrier concentration (n_{ieSiGe}) at base-emitter and base-collector junction for uniform, exponential and Gaussian base doping profiles while varying y_C (0.01 ~0.3) and fixed y_E (0.01). Line (solid, dash, dash-dot) shows n_{ieSiGe} at base-collector junction and symbol (circular, rectangular and star) shows n_{ieSiGe} at base-emitter junction. In the figure x=0 denotes base-emitter junction and x=W_B denotes base-collector junction. From Fig. 4.2a it can be observed that for uniform base doping profile with increasing of y_C, n_{ieSiGe} increases at the base-collector junction exponentially but at base-emitter junction it has no changes. The value of n_{ieSiGe} at both junctions is same while y_C is low (0.01). From Fig. 4.2b it is found that for exponential base doping profile n_{ieSiGe} also increases exponentially with y_C at base-collector junction but it remains same at base-emitter junction. n_{ieSiGe} is smaller at base-collector junction than base-emitter junction while $y_C=y_{E=}0.01$. The scenario of n_{ieSiGe} at both junction for exponential and Gaussian base doping profile is same which depicts at Fig. 4.2c. Though the concentration of n_{ieSiGe} is same at base-collector junction for exponential and Gaussian base doping profile and also same at base-emitter junction for these two profiles, but it is not same between the two junctions throughout the base region (Fig. 4.1d). Fig. 4.2d shows a relative comparison for all three types of profile. It can be observed from Fig. 4.2d that n_{ieSiGe} at base-collector junction for uniform base doping profile is much greater than exponential and Gaussian base doping profile. Although BGN for all three types of profiles is same at base-collector junction for each y_C, n_{ieSiGe} is greater for uniform base doping profile than other two profiles due to only difference in base doping profile. At base-emitter junction n_{ieSiGe} is always same because base doping and BGN both are same at this junction for all three types of profiles. Fig. 4.2d shows that by increasing y_C from 0 to 0.3 without increasing N_B which results about fifteen times more n_{ieSiGe}. It can be also seen that by increasing N_B hundred times without increasing y_C which results n_{ieSiGe} to be increased by seven times.
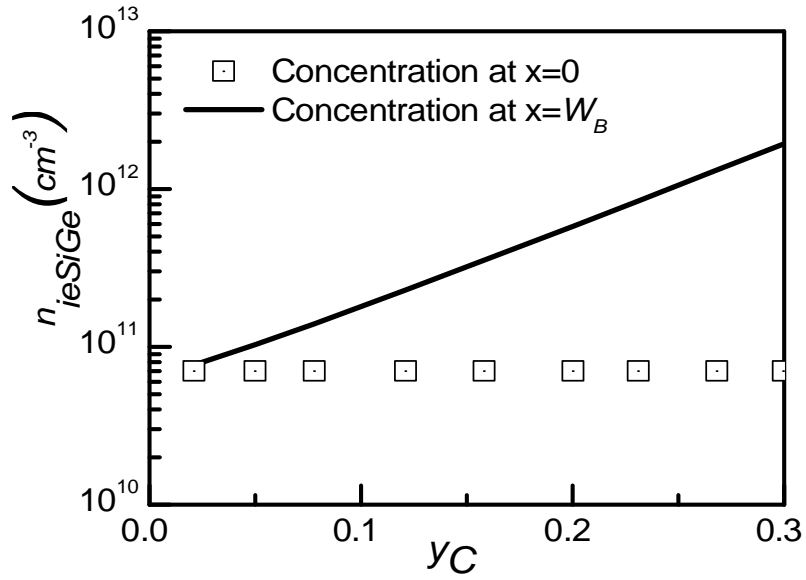
Fig. 4.2a: Intrinsic carrier concentration at base-emitter junction (x=0) and base-collector junction (x=W_B) for varying y_C at uniform base doping profile. Line shows n_{ieSiGe} at base collector junction and symbol shows n_{ieSiGe} at base emitter junction. In both case y_E=0.01.
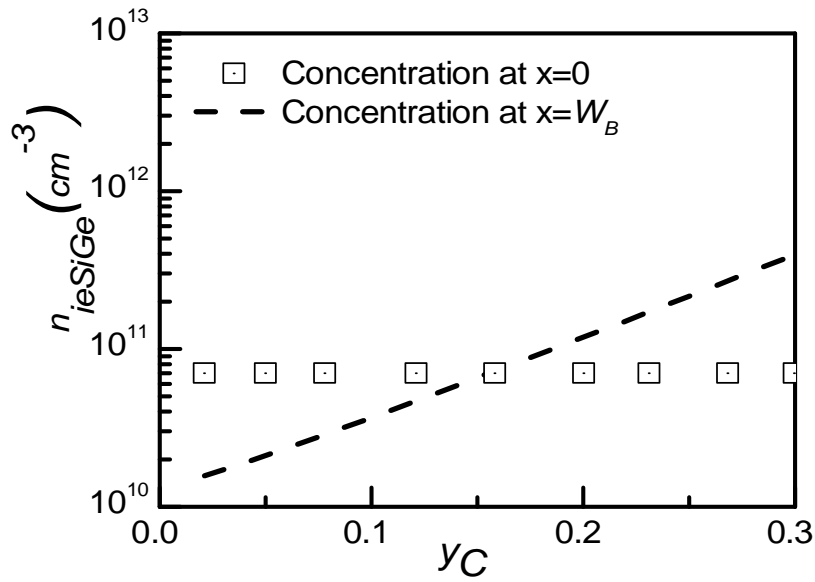
Fig. 4.2b: Intrinsic carrier concentration at base-emitter junction (x=0) and base-collector junction (x=W_B) for varying y_C at exponential base doping profile. Line shows n_{ieSiGe} at base collector junction and symbol shows n_{ieSiGe} at base emitter junction. In both case y_E=0.01.
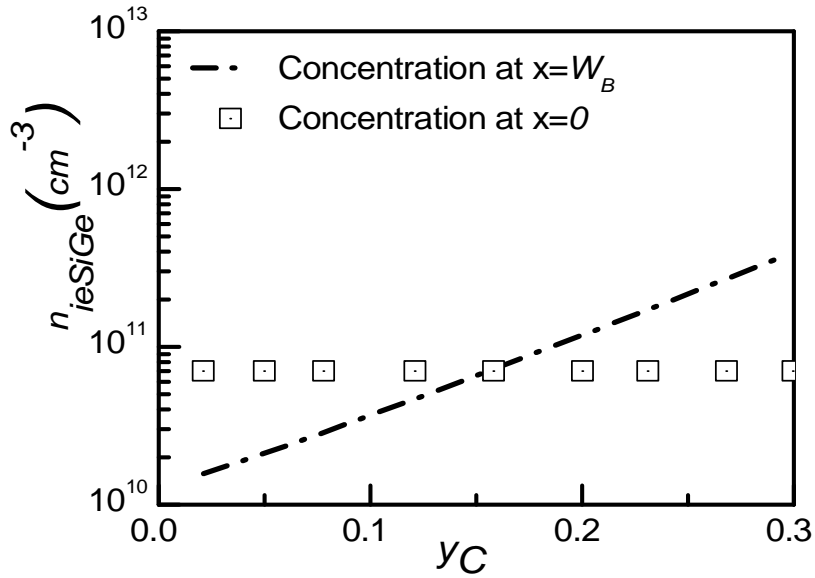
Fig. 4.2c: Intrinsic carrier concentration at base-emitter junction (x=0) and base-collector junction (x=W$_B$) for varying y_C at Gaussian base doping profile. Line shows n_{ieSiGe} at base collector junction and symbol shows n_{ieSiGe} at base emitter junction. In both case y_E=0.01.
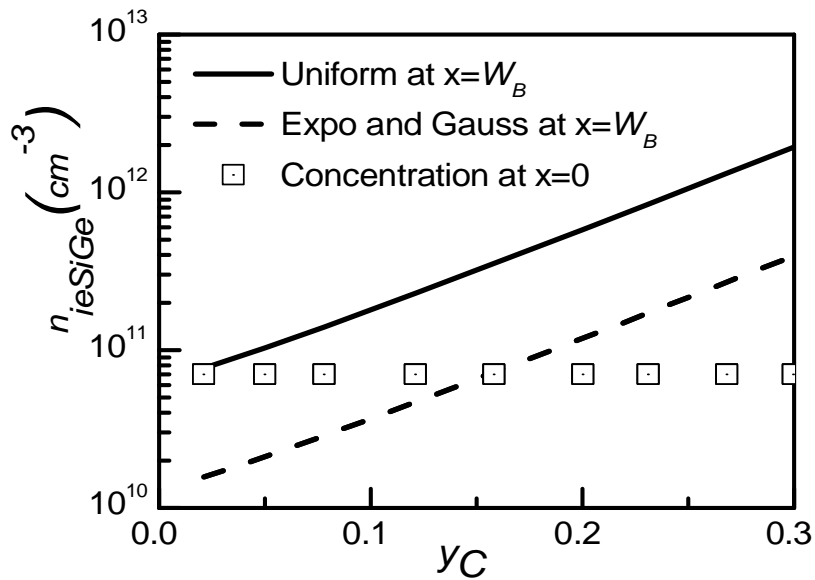

Fig. 4.2d: Intrinsic carrier concentration at base-emitter junction (x=0) and base-collector junction (x=W$_B$) for varying y_C at uniform, exponential and Gaussian base doping profile. Line shows n_{ieSiGe} at base collector junction and symbol shows n_{ieSiGe} at base emitter junction. In both case y_E=0.01.
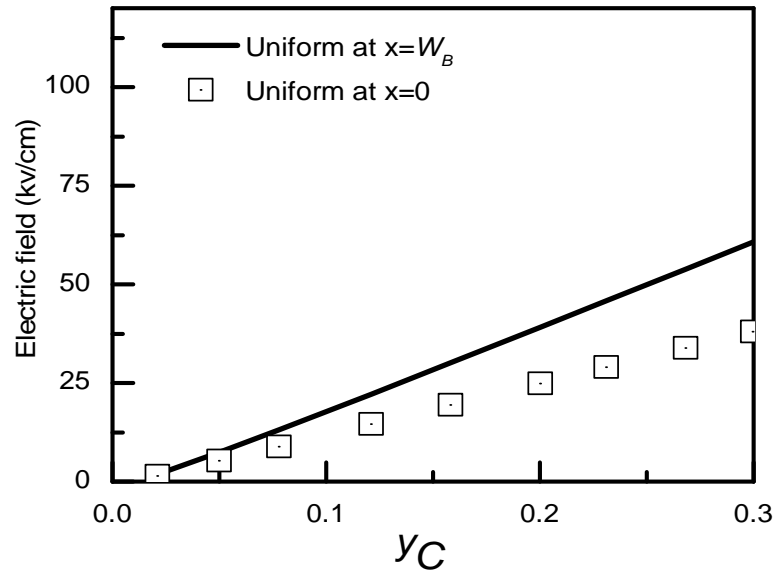
4.2.2 Electric field profile

Fig. 4.3a to Fig. 4.3d shows variation of electric field for three types of base doping profiles with y_C. Line (solid, dash, dash-dot) shows electric field at base-collector junction and symbol (circular, rectangular and star) shows electric field at base-emitter junction. From the earlier discussion it is known that increased germanium enhance BGN (ΔE_{geff}), which increases effective intrinsic carrier concentration (n_{ieSiGe}) exponentially (Fig. 4.2d). From equation (3.16a) it can be observed that, amount of base doping concentration ($N_B(x)$) and n_{ieSiGe} have reverse impact on electric field, but base doping concentration **variation** $\left(\frac{dN_B(x)}{dx}\right)$ and intrinsic carrier concentration variation $\left(\frac{dn_{ieSiGe}(x)}{dx}\right)$ has positive impact on electric field. Fig. 4.3a shows electric field for uniform base doping profile at base-emitter and base-collector junction for fixed y_E and varying y_C. It shows that at both junction electric field increases while y_C increase. Also it can be observed that electric field at base-collector junction is higher than base-emitter junction. The reason can be explained in that way; electric field is proportional to $\left(\frac{dn_{ieSiGe}(x)}{dx}\right)$ and while y_C increases the value of $\left(\frac{dn_{ieSiGe}(x)}{dx}\right)$ is much more higher for base collector junction than base-emitter junction which causes electric filed to be higher at the base-collector junction than base-emitter junction. Fig. 4.3b shows electric field for exponential base doping profile which looks same as uniform base doping profile. Fig. 4.3c shows electric field for Gaussian base doping profile which looks different from uniform and exponential base doping profile.

From Fig. 4.3d comparison for all three types of profiles can be observed. Difference of electric field for Gaussian base doping profile between both junctions is much more than that of uniform and exponential base doping profile. For uniformly doped base (Fig. 4.3a), doping concentration at collector end is 100 times than exponential and Gaussian base doping profile, but it has no variation throughout the base, also n_{ieSiGe} is much more than exponential and Gaussian base doping profile with large variation. All these effects cause electric field lowest for uniform base doping profile than exponential and Gaussian base doping profile at collector end. On the other hand at emitter end base doping and n_{ieSiGe} for all types of profile has same value, but variation of base doping is much more for exponential base doping profile in comparison to other two profiles, so electric field is much higher for exponentially doped base than the other two profiles at the base-emitter

junction. For the same reason electric field is higher for Gaussian base doping profile than other two profiles at the base-collector junction. This built in electric field difference between base-collector junction and base-emitter junction $(E_{lSiGe}(W_B)-E_{lSiGe}(0)$ has significant impact on electron speed, electron will take smaller time if the value is higher while passing through base region. For high speed circuit design it plays an important role, as base transit time is the main determining factor for maximum oscillation frequency.

Fig. 4.3a: Electric field at base-collector junction, $E_{lSiGe}(W_B)$ (Line) and base-emitter junction, $E_{lSiGe}(0)$ (symbol) for $y_E=0.01$ and varying y_C (0.01~0.3) for uniform doping profile.
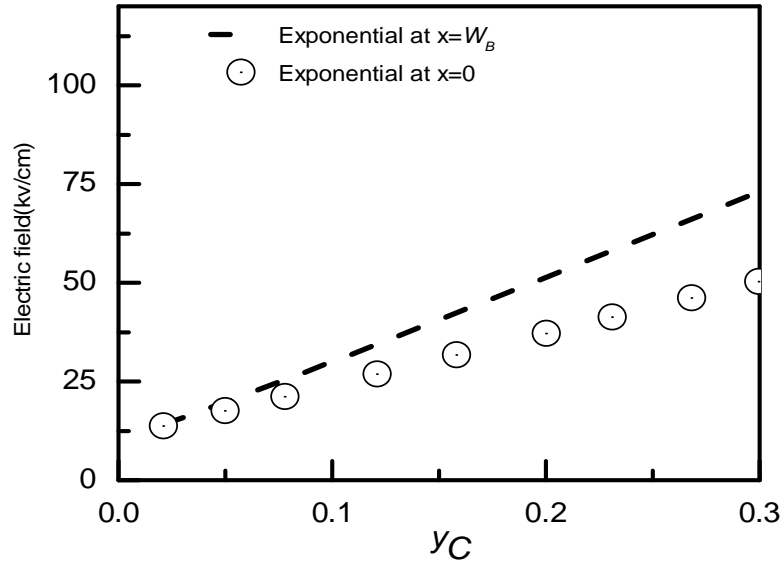
Fig. 4.3b: Electric field at base-collector junction, $E_{lSiGe}(W_B)$ (Line) and base-emitter junction, $E_{lSiGe}(0)$ (symbol) for y_E=0.01 and varying y_C (0.01~0.3) for exponential doping profile.
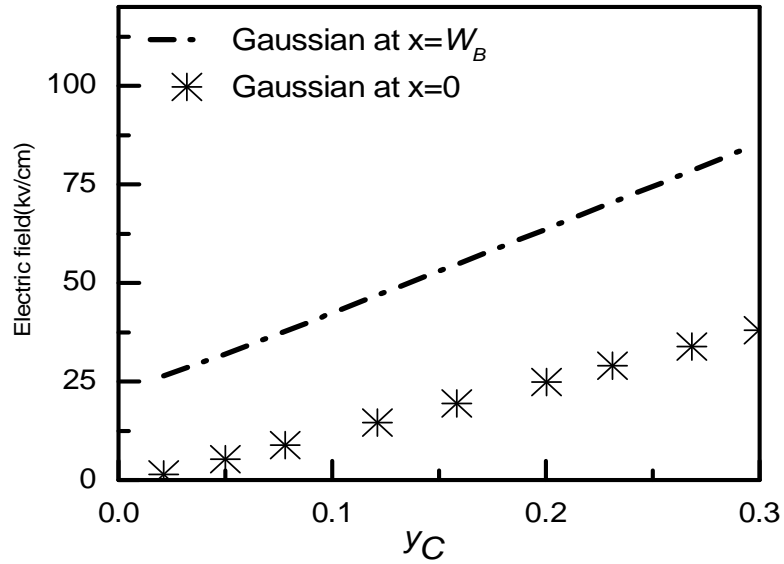
Fig. 4.3c: Electric field at base-collector junction, $E_{lSiGe}(W_B)$ (Line) and base-emitter junction, $E_{lSiGe}(0)$ (symbol) for y_E=0.01 and varying y_C (0.01~0.3) for Gaussian doping profile.
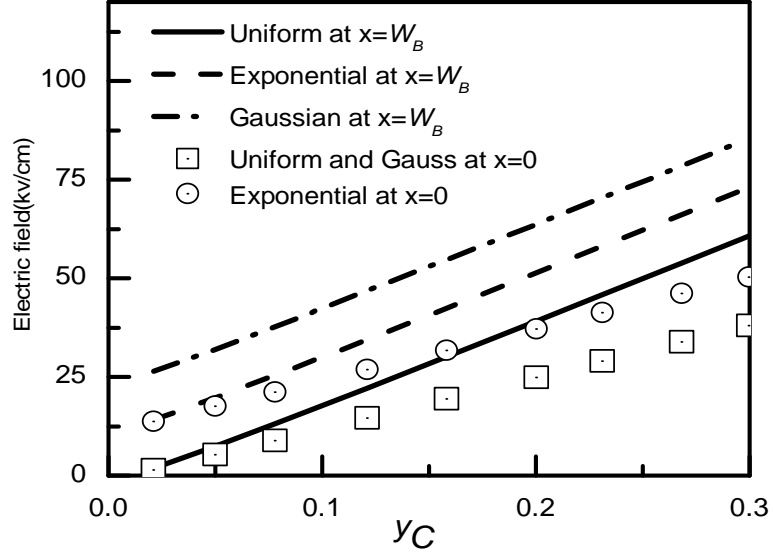
Fig. 4.3d: Electric field at base-collector junction, $E_{lSiGe}(W_B)$ (Line) and base-emitter junction, $E_{lSiGe}(0)$ (symbol) for y_E=0.01 and varying y_C (0.01~0.3) for three types of doping profiles.

4.2.3 Diffusivity profile

Fig. 4.4a to Fig. 4.4d shows diffusivity for three types of base doping profiles at base-collector junction. Here y_E is fixed at 0.01 and y_C is varied (0.01 to 0.3). Line (solid, dash, dash-dot) shows diffusivity considering velocity saturation (v_s) effect and symbol (rectangular, circular and star) shows diffusivity without considering v_s effect. Fig. 4.4a shows diffusivity for uniform base doping profile at base collector junction. Here it is found that for uniform base doping profile diffusivity have no significant changes while variation of y_C. v_s also has no significant effect on diffusivity. For exponential base doping profile, the diffusivity decreases sharply with y_C (Fig. 4.4b). v_s also has significant effect on exponential base doping profile and no significant effect observed for Gaussian base doping profile (Fig. 4.4c). Comparison for all three types of profiles can be observed from Fig. 4.4d. Due to increasing electric field and velocity saturation, diffusivity reduces in the base region with the increase of y_C. For uniform base doping profile variation of diffusivity with y_C is less than exponential and Gaussian base doping profile because the variation of effective intrinsic carrier concentration (n_{ieSiGe}) for uniform base doping

profile is less at collector-base junction in compared to exponential and Gaussian base doping profile. As diffusivity and mobility are related among them by a constant multiplying factor so diffusivity signifies mobility of electron.
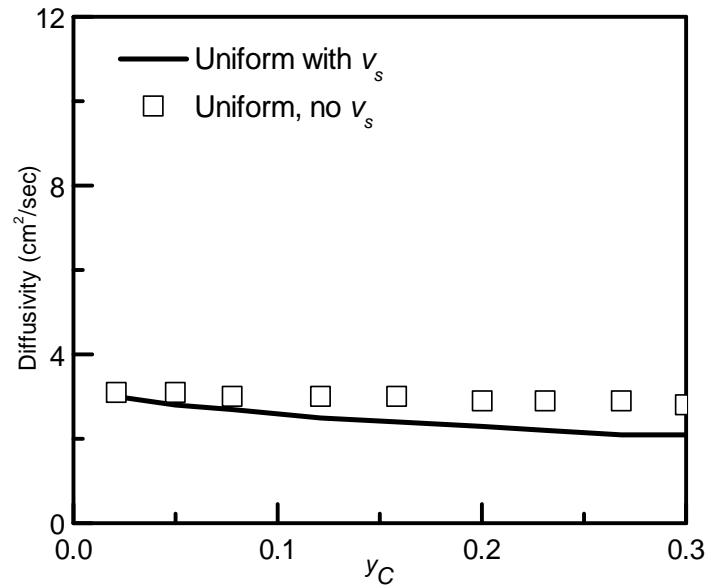
Fig. 4.4a: Diffusion coefficient at base-collector junction, $D_{nSiGe}(W_B)$ considering velocity saturation (line) and without velocity saturation (symbol) for $y_E=0.01$ and varying y_C for uniform base doping profile.
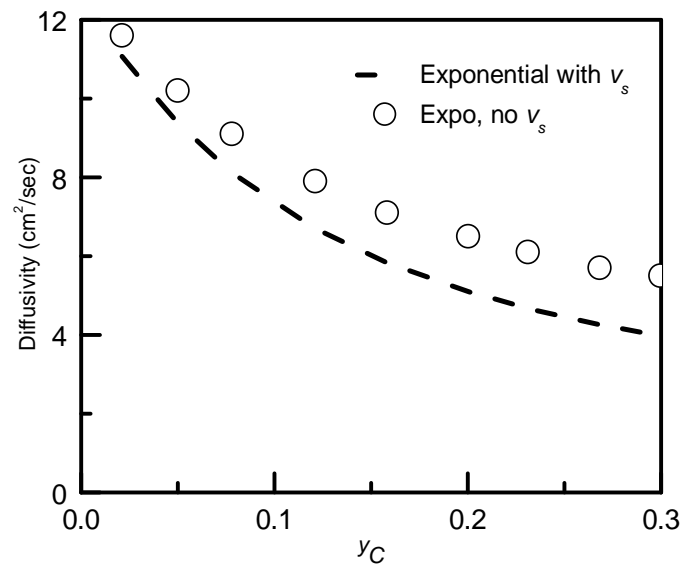
Fig. 4.4b: Diffusion coefficient at base-collector junction, $D_{nSiGe}(W_B)$ considering velocity saturation (line) and without velocity saturation (symbol) for $y_E=0.01$ and varying y_C for exponential base doping profile.
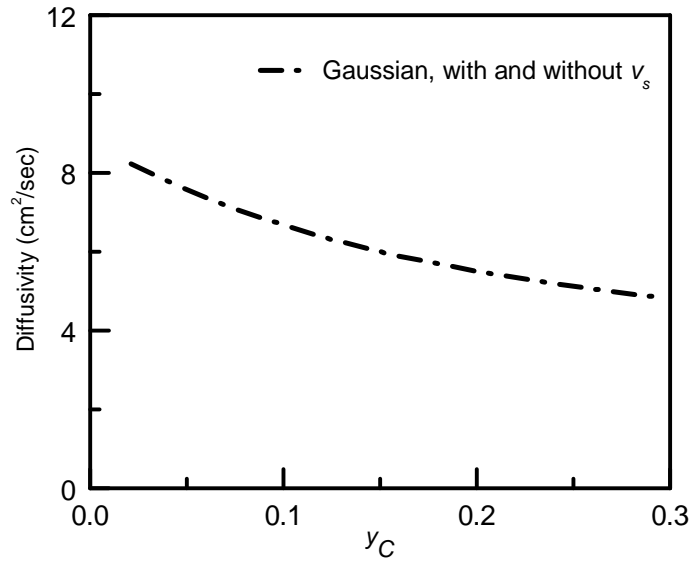
Fig. 4.4c: Diffusion coefficient at base-collector junction, $D_{nSiGe}(W_B)$ considering velocity saturation and without velocity saturation for y_E=0.01 and varying y_C for Gaussian base doping profile.
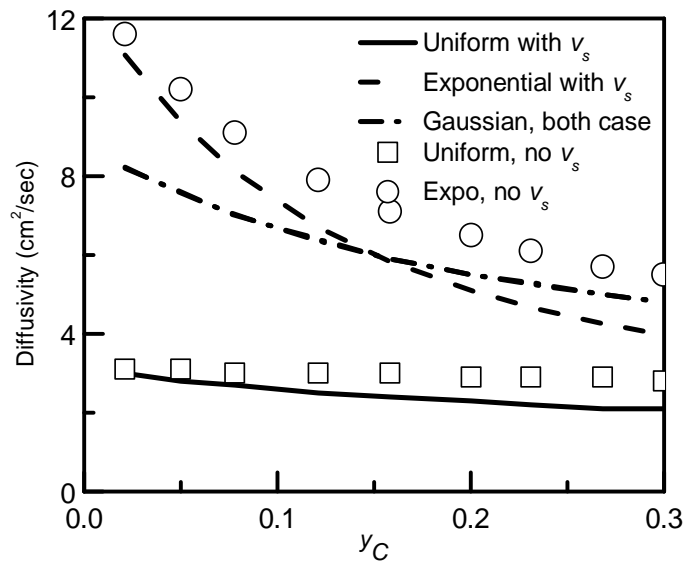
Fig. 4.4d: Diffusion coefficient at base-collector junction, $D_{nSiGe}(W_B)$ considering velocity saturation (line) and without velocity saturation (symbol) for y_E=0.01 and varying y_C for three types of doping profiles.

4.2.4 Early voltage profile

Fig. 4.5a to Fig. 4.5e shows Early voltage for fixed y_E (=0.01) and varying y_C (0.01~0.3). Early voltage increases exponentially with y_C. Base width, W_B is 300Å, peak doping at base-emitter junction is 10^{19} cm^{-3} and minimum doping at base-collector junction is 10^{17} cm^{-3} for Gaussian and exponential base doping profiles, 10^{19} cm^{-3} considered for uniform based doping profile. Fig. 4.5a shows Early voltage for uniform base doping profile which increases exponentially with y_C. V_A increases almost 500 times by increasing y_C from 0.01 to 0.3 for uniform base doping profile. Fig. 4.5b shows Early voltage for exponential base doping profile and Fig. 4.5c shows V_A for Gaussian base doping profile. For all three types of profiles V_A profile is similar. A comparison for all three types of profiles is shown in Fig. 4.5d. If effective intrinsic carrier concentration at the base-collector junction, $n_{ieSiGe}(W_B)$ increases, it increases Early voltage (3.18b). $n_{ieSiGe}(W_B)$ for uniformly doped base is greater than Gaussian and exponentially doped base (Fig. 4.1d), so V_A for uniform base doping profile is greater than exponential and Gaussian base doping profile. It is also found that V_A is greater for exponential base doping profile than Gaussian base doping profile although $n_{ieSiGe}(W_B)$ is same for both doping profiles. Actually Early voltage increases proportionally with the increase of $n_{ieSiGe}(W_B)$, but it has a inverse relation with total amount of n_{ieSiGe} content in the base (3.18b). Total amount of n_{ieSiGe} is greater for Gaussian than exponential base doping profile (Fig. 4.1d), and for this reason Early voltage is greater for exponentially doped base than Gaussian base doping profile.

Part of our Result (Gaussian base doping profile) compared with [19] (triangular symbol used in Fig. 4.5e) and found in good agreement for V_A.

Fig. 4.6 shows Early voltage for varying y_E with fixed y_C at 0.3. Here it is observed that by increasing y_E, V_A reduces exponentially for three types of base doping profiles. While y_E is increased, this results has no significant variation in $n_{ieSiGe}(W_B)$, but it increases n_{ieSiGe} throughout the base region. If $n_{ieSiGe}(W_B)$ is fixed but n_{ieSiGe} increases in the base region while increasing y_E, it reduces V_A (3.18b), which also explained in the previous sections. While y_E is nearly 0, this profile is triangular germanium profile, V_A in this profile is maximum. For other value of y_E germanium profile is trapezoidal. In this case

V_A reduces gradually. When $y_E = y_C = 0.3$, this shows box germanium profile, in this case V_A is minimum.
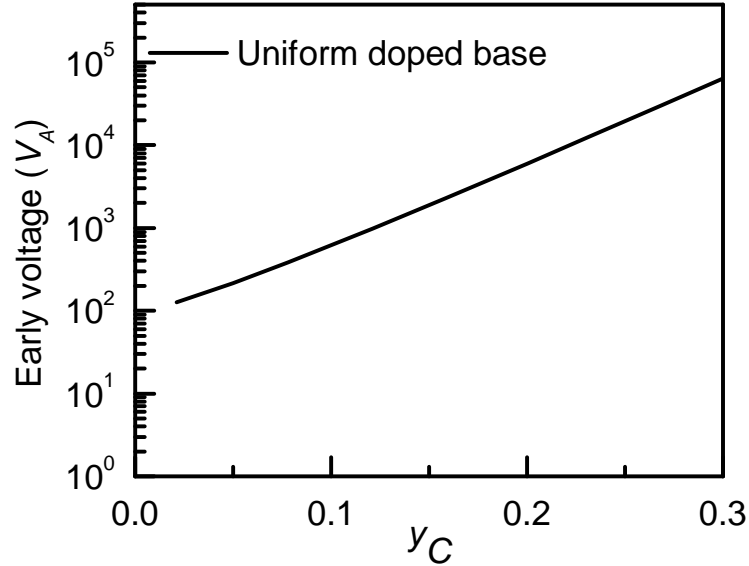
Fig. 4.5a: Early voltages for y_E=0.01 and varying y_C for uniform base doping profile. Base width, W_B is 300Å, base doping is 10^{19} cm^{-3}.
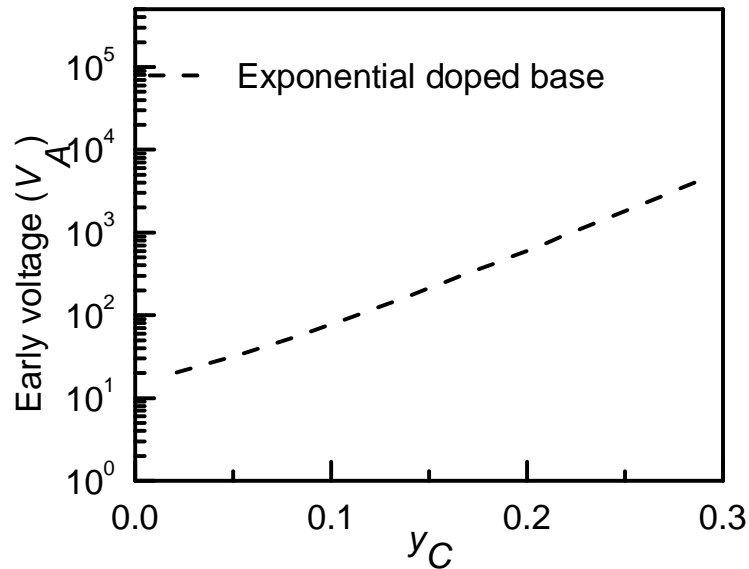
Fig. 4.5b: Early voltages for y_E=0.01 and varying y_C for exponential base doping profile. Base width, W_B is 300Å, peak doping at base-emitter junction is 10^{19} cm^{-3} and minimum doping at base-collector junction is 10^{17} cm^{-3}.
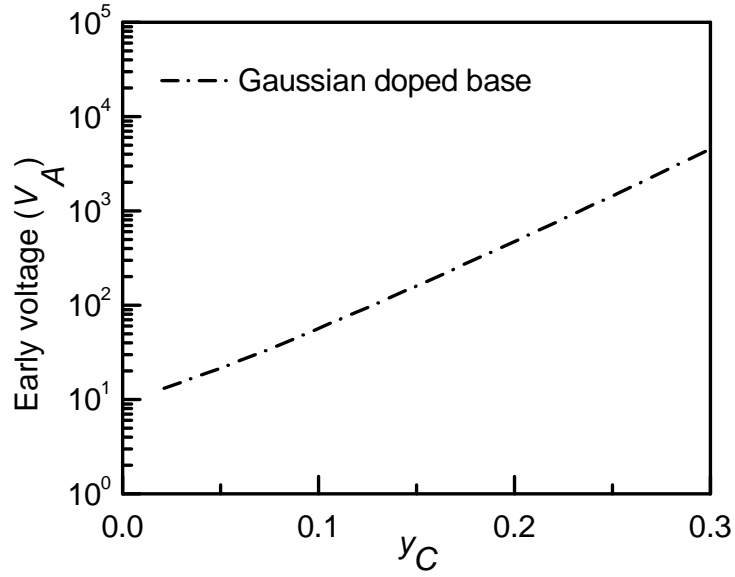
Fig. 4.5c: Early voltages for y_E=0.01 and varying y_C for Gaussian base doping profile. Base width, W_B is 300Å, peak doping at base-emitter junction is 10^{19} cm^{-3} and minimum doping at base-collector junction is 10^{17} cm^{-3}.
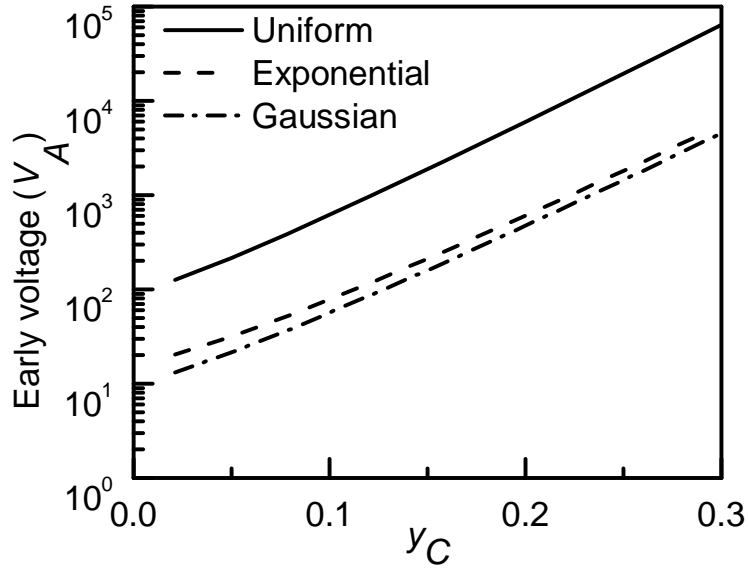
Fig. 4.5d: Early voltages for y_E=0.01 and varying y_C for Gaussian, exponential and uniform base doping profiles. Base width, W_B is 300Å, peak doping at base-emitter junction is 10^{19} cm^{-3} and minimum doping at base-collector junction is 10^{17} cm^{-3} for Gaussian and exponential base profiles, 10^{19} cm^{-3} considered for uniform based doping profile.
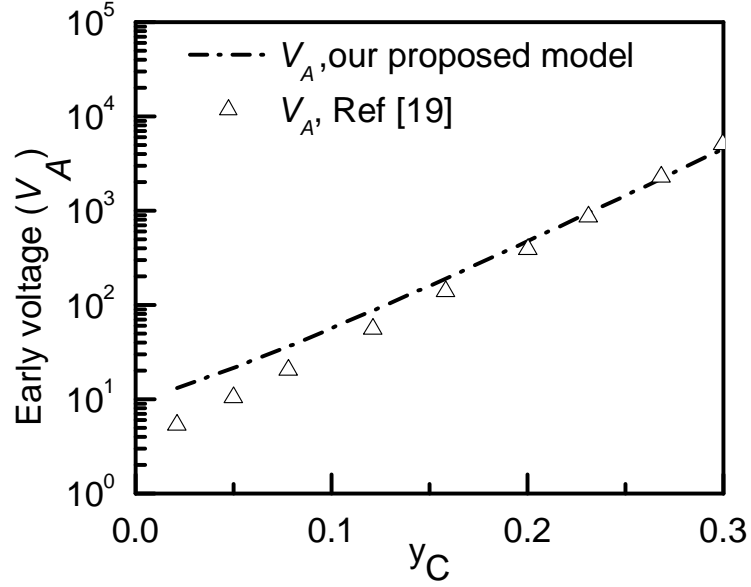
Fig. 4.5e: Early voltages for y_E=0.01 and varying y_C for Gaussian doped profile with our proposed model and result in the previous literature [19]. Base width, W_B is 300Å, peak doping at base-emitter junction is 10^{19} cm^{-3} and minimum doping at base-collector junction is 10^{17} cm^{-3}.
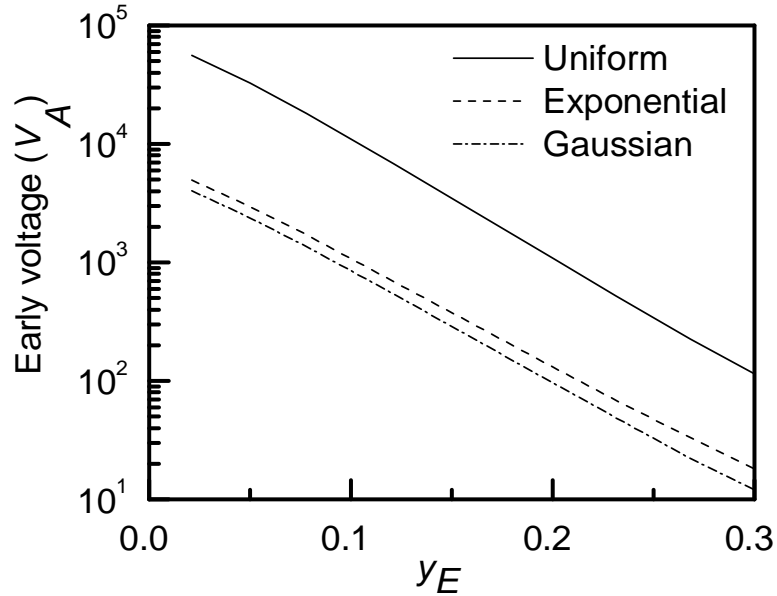
Fig. 4.6: Early voltage for y_C=0.3 and varying y_E for Gaussian, exponential and uniform base doping profiles. Base width, W_B is 300Å, peak doping at base-emitter junction is 10^{19} cm^{-3} and minimum doping at base-collector junction is 10^{17} cm^{-3}.

Fig. 4.7a shows doping concentration dependency of V_A for three types of doping profiles. Here it is observed that V_A is proportional to doping concentration. For exponential and Gaussian profiles for each $N_B(0)$, $N_B(0)/N_B(W_B)$ is kept constant at 100. Also it can be observed that Early voltage for exponential base doping profile is higher than Gaussian base doping profile for same $N_B(0)$. The process which reduces Early effect can increase Early voltage, which discussed at Section 1.4. For a certain base doping concentration and reverse biased collector base voltage how much depletion region creates in the base, it reduces by the overall increase of base doping concentration as well as Early effect also reduces. For that reason increasing doping concentration increases Early voltage.

Fig. 4.7b shows variation of V_A with exponential co-efficient m_{exp} for exponential base doping profile. Variation of m_{exp} is done by varying $N_B(W)$. From (3.12a) it is found that when $N_B(W_B)$ decreases from it's maximum value which initial value was $N_B(0)$, m_{exp} increase as well as V_A decrease.
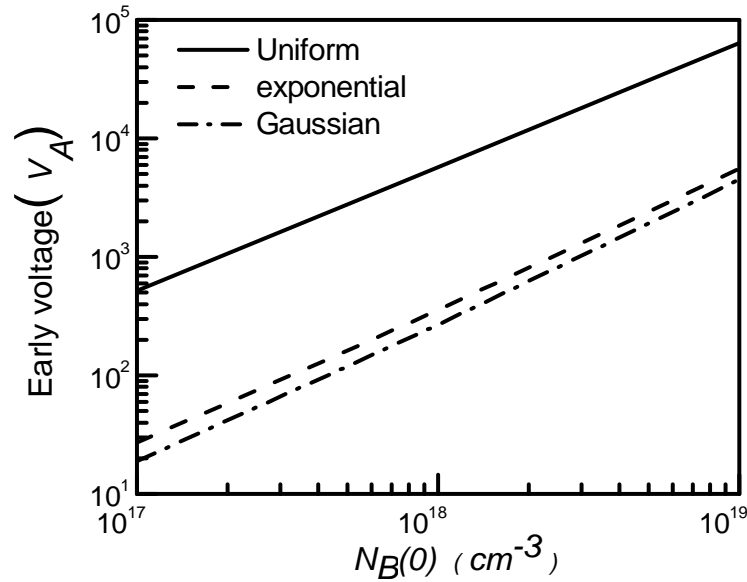
Fig. 4.7a: Early voltage (V_A) for triangular germanium profile with $y_C=0.3$ and $y_E=0.01$ with varying base doping. Doping concentration at base-collector junction for uniform doped $N_B(W_B)=N_B(0)$ and for exponential and Gaussian doped $N_B(W_B)=N_B(0)/100$.
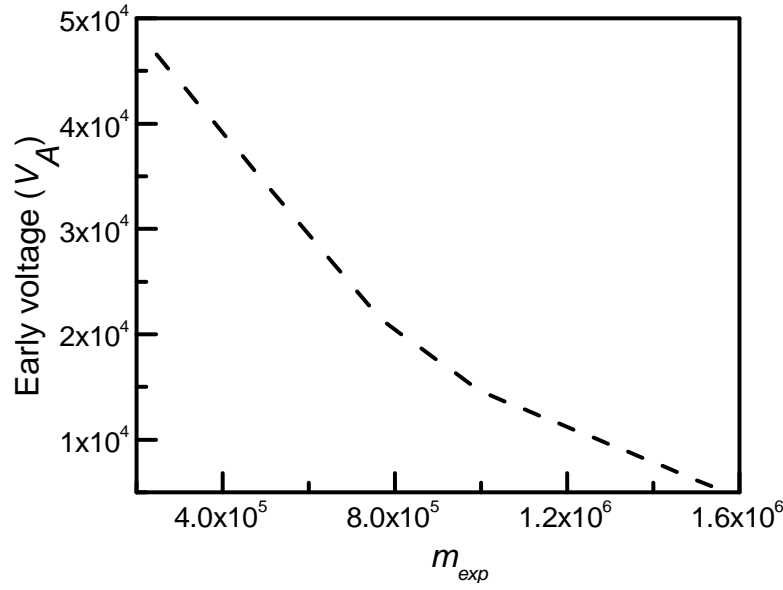
Fig. 4.7b: Early voltage (V_A) for exponential doping profile with the variation of m_{exp}

4.2.5 Collector saturation current density (J_{CO}) and common emitter current gain (β)

Fig. 4.8a to Fig. 4.8d shows dependence of collector saturation current density for uniform, exponential and Gaussian base doping profiles with varying y_C and fixed y_E at 0.01. Line (solid, dash, dash-dot) denotes J_{CO} considering electron velocity saturation effect (v_s) and symbol (rectangular, circular) denotes J_{CO} by ignoring v_s. For Gaussian and exponential base doping profile, J_{CO} decrease as y_C increases. From Fig 4.8a it can be observed that for uniform base doping profile J_{CO} decreases with the increase of y_C after slightly increasing with y_C. This decreasing of J_{CO} is true for both considering v_s and ignoring that. Fig. 4.8b denotes J_{CO} for exponential base doping profile. Here it is observed that if v_S is considered, J_{CO} decreases with y_C but if v_S is ignored, J_{CO} increases with y_C. It can be explained that in exponential base doping profile electron velocity reaches it's saturation value before reaching base-collector junction. If we avoid v_S in our calculation , theoretically its velocity increase as well as J_{CO} also increases but if v_S is considered than electron velocity cannot overcome v_S and J_{CO} decreases. Fig. 4.8C denotes J_{CO} for Gaussian base doping profile where v_S has no real impact on J_{CO}.

Fig. 4.8d provides a comparison report for three types of base doping profiles where it can be seen that for exponential base doping profile J_{CO} is minimum. Collector current depends on quantity of intrinsic carrier concentration (n_{ieSiGe}) as well as gradient of intrinsic carrier concentration (Δn_{ieSiGe}) and diffusivity (D_{nSiGe}). $n_{ieSiGe}(0)$ and $n_{ieSiGe}(W_B)$ for exponential base doping profile is the same as $n_{ieSiGe}(0)$ and $n_{ieSiGe}(W_B)$ for Gaussian base doping profile, but total amount of n_{ieSiGe} in the base is not same for these two doping profile (Fig. 4.1). The quantity of n_{ieSiGe} is greater for Gaussian base doping profile, so J_{CO} is greater for Gaussian base doping profile than exponential base doping profile.

Electron mobility decreases when electric field increases (Fig. 4.3d & 4.4d). Electric field increases exponentially as y_C increases and electric field is maximum at the base-collector junction (Fig. 4.4d). Due to high electric field, mobility near the collector base junction decreases, which results electron cannot reach saturation speed. Velocity saturation makes no real difference in collector current for Gaussian base doping profile, but it has significant impact for uniform and exponential base doping profiles (Fig.4.8d) [71][72].
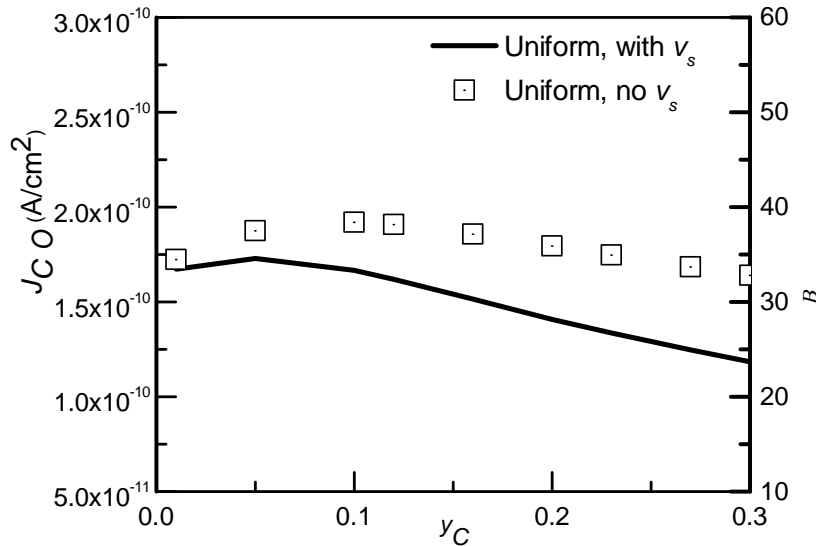
Fig. 4.8a: Collector saturation current density (J_{CO}) for fixed y_E (0.01) and varying y_C for uniform base doping profile. Line shows J_{CO} considering v_s and symbol shows J_{CO} ignoring v_s. Right side of figure shows common emitter current gain *(β)* considering J_{BO}= 5 pA/cm^2.
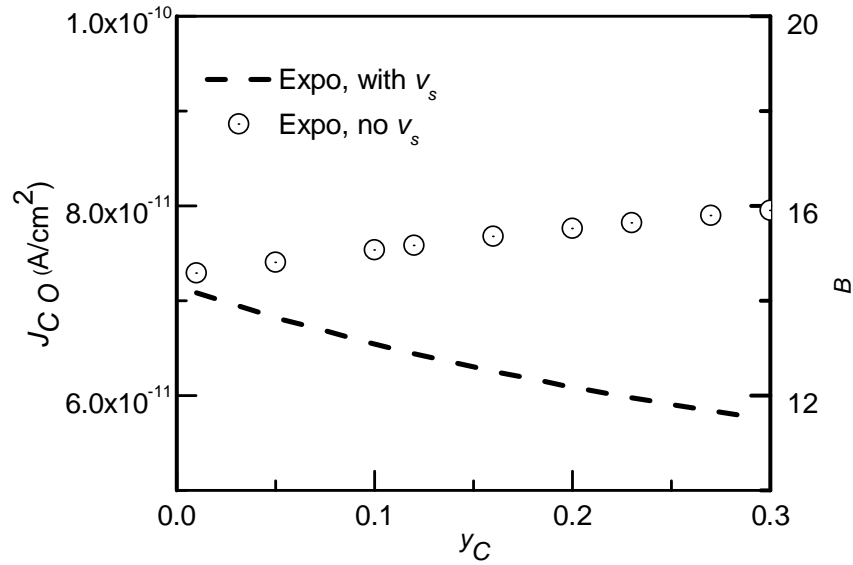
Fig. 4.8b: Collector saturation current density (J_{CO}) for fixed y_E (0.01) and varying y_C for exponential base doping profile. Line shows J_{CO} considering v_s and symbol shows J_{CO} ignoring v_s. Right side of figure shows common emitter current gain *(β)* considering J_{BO}= 5 pA/cm^2.
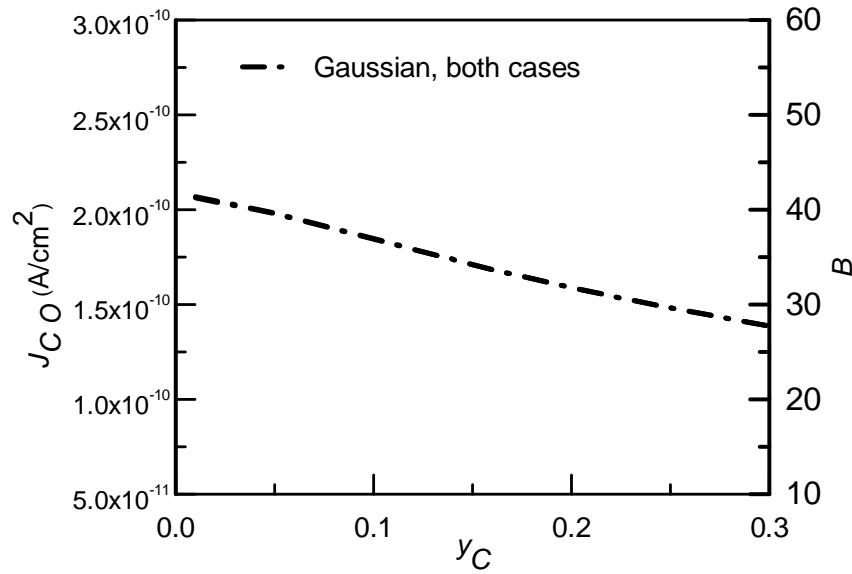
Fig. 4.8c: Collector saturation current density (J_{CO}) for fixed y_E (0.01) and varying y_C for Gaussian base doping profile. Line shows J_{CO} considering v_s and symbol shows J_{CO} ignoring v_s. Right side of figure shows common emitter current gain *(β)* considering J_{BO}= 5 pA/cm^2.
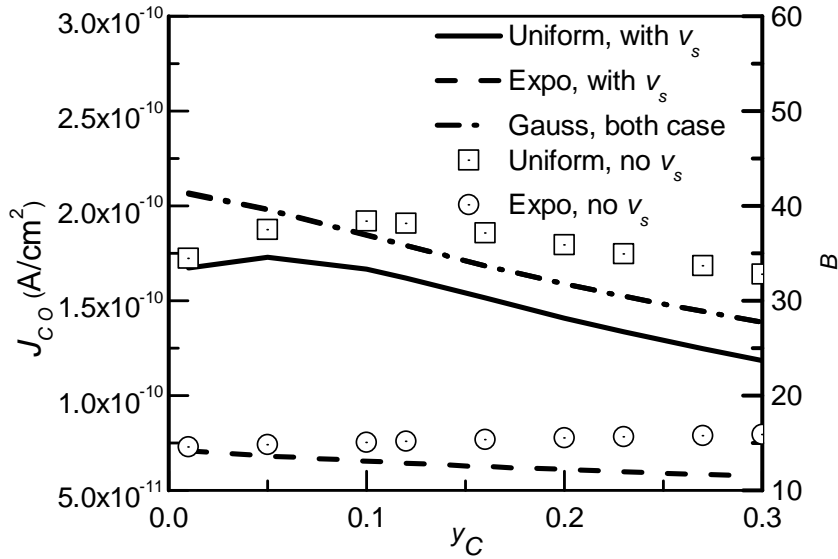
Fig. 4.8d: Collector saturation current density (J_{CO}) for fixed y_E (0.01) and varying y_C for three types of base doping profiles. Line shows J_{CO} considering v_s and symbol shows J_{CO} ignoring v_s. Right side of figure shows common emitter current gain *(β)* considering J_{BO}= 5 pA/cm^2.

Fig. 4.9 shows common emitter current gain *(β)* for varying y_C and fixed y_E at 0.15. It has been observed that *β* increases while y_C increases for Gaussian and uniformly doped base but after certain value of y_C it starts reducing. For an *n-p-n* transistor electron enters through emitter and major parts of it pass towards collector with negligible loss in base region due to electron hole recombination. When y_C is small (~0.01) and y_E~0.15, electron concentration is maximum near base-emitter junction and gradually decreases towards base-collector junction. While y_C increases electron concentration increases in the base-collector junction which causes J_{CO} as well as *β* to be increased. After certain y_C (~0.15), electron concentration in collector-base junction is more than base-emitter junction which causes diffusion effect in the reverse direction to the normal electron flow from emitter to collector. Moreover diffusivity also reduces by increasing y_C .These two effects decrease J_{CO} as well as *β*. But for exponentially doped base *β* starts decreasing while y_C increases.
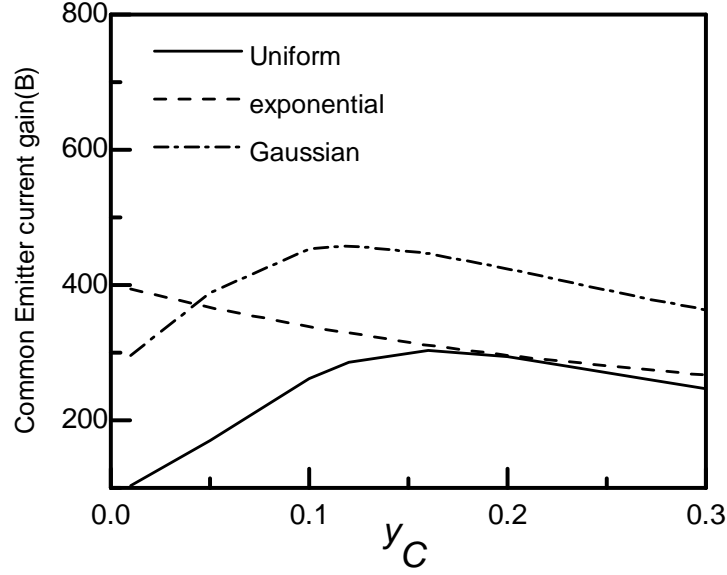
Fig. 4.9: Common emitter current gain *(β)* for y_E =0.15 and varying y_C for uniform, exponential and Gaussian base doping profile. J_{BO} is considered 5 pA/cm^2.

Table 4.1

Calculated value showing current gain and Early voltage of SiGe HBT for various y_C and y_E combinations.

Ge-mole fraction		Uniform base doping profile		Exponential base doping profile		Gaussian base doping profile	
y_E	y_C	V_A	$β$	V_A	$β$	V_A	$β$
0.01	0.01	18	111	379	39	11	39
0.01	0.14	92	111	1937	29	64	35
0.01	0.25	980	85	17446	24	643	30
0.14	0.01	10	239	88	355	8	198
0.14	0.14	15	884	378	256	11	357
0.14	0.25	137	748	2880	202	89	312
0.25	0.01	15	240	-30	3551	-4	309
0.25	0.14	6	3112	122	3339	4	2769
0.25	0.25	15	9338	378	2618	11	4213

Table 4.1 shows calculated value of *β*, V_A for 9 different devices containing various Germanium profiles at the base. For all these devices, J_{BO} = 5pA/cm^2, W_B= 400Å, $N_B(0)$ =10^{19} cm^{-3}, $N_B(W_B)$=10^{17} cm^{-3} for Gaussian and exponentially doped base. It is

59

observed that for Gaussian and uniform doping profiles, if $(y_C \geq y_E)$ and $(y_C - y_E)$ increases by varying either y_C or y_E, β decreases gradually but V_A increases. Conversely it can say that if $(y_C \leq y_E)$ and $(y_E - y_C)$ increases by varying either y_C or y_E, β increases gradually but V_A decreases. Variation of β for trapezoidal and triangular germanium profiles can be explained by the above statements. For box germanium profile, increment of germanium has no significant change on V_A, but it increases β significantly. Increment of both y_C and y_E reduces diffusivity but it increase intrinsic carrier concentration throughout the base region, which causes β to increase for box germanium profile by increasing germanium content.

Table 4.2

Comparison of V_A and β with [75] and our proposed model

Ge-mole fraction		Uniform base doping profile		Ref [75]	
y_E	y_C	V_A	β	V_A	β
0.14	0.14	15	803	18	750
0.25	0.14	6	1730	6	1800
0.14	0.25	137	1244	120	1400
0.25	0.25	15	2335	44	1750

Table 4.2 shows part of this result (only uniform base doping profile with trapezoidal germanium profile) which compared with [75]. Here it is found that V_A and β is in good match with [75].

4.2.6 Cutoff frequency

In recent years, the demand for high-speed transistors is increasing due to the bandwidth required by telecommunication systems. In the past, the application of Si-based technology has been believed to be limited up to 10 Gbps systems mainly due to its operation speed limit, despite the advantages such as high reliability, low cost, and the high level of integration over GaAs and InP technologies. Recently, the 120 GHz f_T SiGe BiCMOS technology has been developed for the 40 Gbps communication system [76]. Fig. 4.10 shows frequency response of HBT device with emitter area $A_E=0.3 \times 10.16 \mu m^2$ with uniform based doped with respect to collector current. This result is compared with practical HBT device [74].
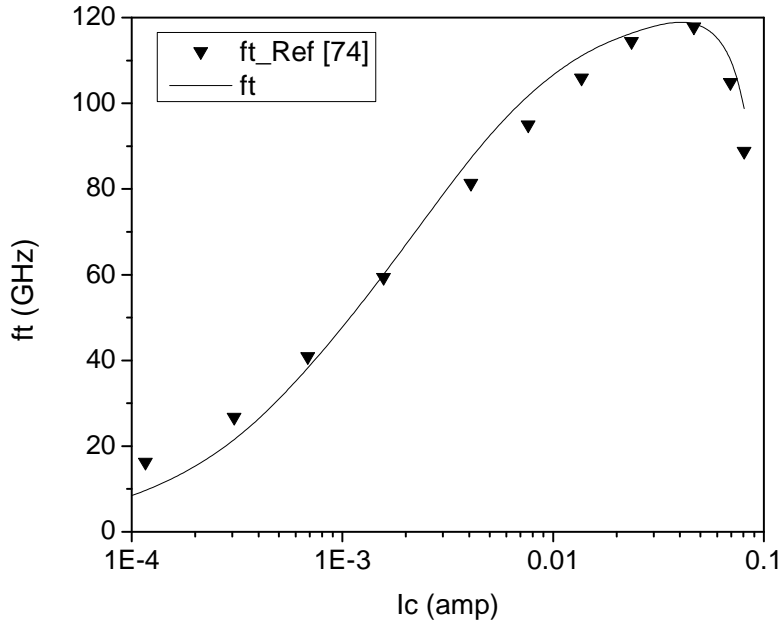
Fig. 4.10: Frequency response of HBT with respect to collector current.

4.3 CONCLUSION

The analytical expression obtained in chapter three was used to determine the effects of various parameters on Early voltage (V_A), Common emitter current gain (β) and cut-off frequency (f_T). Here it is observed that V_A and β are highly dependent on Ge-mole fraction. Electron velocity saturation effect (v_s) observed on diffusivity and collector current density (J_{CO}). It is found that v_s has significant impact on both J_{CO} and diffusivity for uniform and exponential base doping profiles; for Gaussian base doping profile it impact is negligible. f_T of HBT is also dependent on collector current; increasing collector current increases cut-off frequency. But after certain range of collector current f_T starts reducing due to parasitic capacitance increases.

CHAPTER 5

CONCLUSION AND SUGGESTIONS

5.1 CONCLUSION

In the present work, closed form analytical model were derived for early voltage (V_A) and common emitter current gain (β) for uniform, exponential and Gaussian base doping profiles with trapezoidal/triangular/box Germanium profiles heterojunction bipolar transistor (HBT). Field dependent mobility, doping dependent mobility, band gap narrowing (BGN) (due to both heavy doping and presence of Germanium content in the base) and velocity saturation effects were considered in this model. The effects of base doping profile and Germanium profile on V_A and β observed in this work. Effects of Ge mole fraction on diffusivity (D_{nSiGe}), effective intrinsic carrier concentration (n_{ieSiGe}) and electric field (E_{lSiGe}) were studied. Electron velocity saturation effect (v_s) was studied on diffusivity and collector saturation current density (J_{CO}). It is found that v_s has significant impact on both J_{CO} and diffusivity for uniform and exponential base doping profiles; for Gaussian base doping profile it impact is negligible. Cutoff frequency for HBT calculated in this work. The results obtained by using this analytical model compared with the results available in the previous literature and found in good agreement.

5.2 SUGGESTIONS FOR FUTURE WORK

In this work, three different base doping profiles (uniform, exponential and Gaussian) with arbitrary Germanium profiles were considered. For these profiles analytical modeling of Early voltage (V_A) and common emitter current gain (β) were derived considering field dependent mobility, doping dependent mobility, band gap narrowing (BGN), changes in density of state (DOS) and velocity saturation effect. BGN was considered due to heavy doping and presence of Germanium. The variations of V_A and β for various base doping profiles and germanium profiles were addressed. Cut off frequency also calculated by using this model.

Base transit time is an important factor for semiconductor devices. Although this model is used for V_A and β calculation, this can also be used to calculate base transit time which is an important factor for high speed device design.

The HBT considered here was a SiGe based heterojunction bipolar transistor. Attempt should be taken to investigate Early voltage (V_A), current gain (β) cut-off frequency (f_T) using this model for InP, AlGaAs etc based HBT.

In this analysis recombination effect is neglected which effect considered ignorable. Further verification need to consider this effect on V_A, β and f_T.

This analysis also valid up to low injection of minority carrier in the base. For high injection this model need to change.

Distortion of energy band at base-emitter and base-collector junction due to band gap engineering need to be considered, which will make possible more accurate result of V_A, β and f_T.

REFERENCES:

[1]   Jaeger, R.C. and Blalock, T.N.,"Microelectronic circuit design",. McGraw-Hill Professional. pp. 317, 2004.

[2]   Alioto, M., and Palumbo, G., "Model and design of bipolar and MOS current-mode logic: CML, ECL and SCL digital circuits" Springer, 2005.

[3]   Antognetti, P. and Massobrio, G., "Semiconductor device modeling with Spice", McGraw-Hill Professional, 1993.

[4]   Ohishi, T., Abe, Y., Sugimoto, H., Ohtsuka K. and Matsui, T., "Ultra high current gain InGaAsP/InP heterojunation biloar transistor", IEEE Electron Device, vol. 26, pp. 392-393, 1990.

[5]   Song, J., Hong, W., Palmstrom, C., Van, B. P. and Chough, K. B., "InP based carbon doped based HBT Technology", IEEE International Electron Device Meeting (IEDM), Washington, D.C., pp. 787-790, 1993.

[6]   Shigenmatsu, H., Iwai, T., Matsumiya, Y., Ohnishi, H., Ueda, O. and Fuji, T., "Microwave power InAlAs/InGaAs double heterojunction bipolar transistor with 1.5 volt low voltage operation", pp 88-89, 1995.

[7]   Tadao, I. and Yamauchi, Y., "A possible near-ballistic collection in an AlGaAs/GaAs HBT with a modified collector structure", IEEE transactions on electron devices, vol. 35, no. 4, 1988.

[8]   Tang, Z. R., Kamins, T., Salama, C. A. T., "Current gain-Early voltage product in SiGe base HBT's with thin θ-Si:H emitters", IEEE Tran. on Electron Devices, pp. 473 - 476, 1994.

[9]   Chiu, S. Y. and Anwar, A. F. M., "Effect of surface recombination on the Early voltage in HBTs", Semicond. Sci. Technol, vol. 14, no. 9, 1999.

[10]   Wang, Y. D., Yang, X., Zhang, H. W., "Effect of base structure optimization of SiGe HBTs on Early voltage**,** Institute of Microelectronics, Tsinghua University,Beijing 100084,P.R.China, 2006.

[11]   Ningyue, J. and Zhenqiang, M., "Current gain of SiGe HBTs under high basedoping concentrations", Semicond. Sci. Technol, vol. 22, no. 1, 2007.

[12]   Prinz, E. J. and Sturm, J. C., "Current gain-Early voltage products in heterojunction bipolar transistors with nonuniform base bandgaps", IEEE Electron Device Letters, vol. 12, no. 12, 1991.

[13]   Yuan, J. S. and Song, J., "Early voltage of SiGe heterojunction bipolar transistor", Electron Devices Meeting, IEEE Honkong, pp. 102-105, 1997.

[14] Eduardo, C. J. and Cortes, F. P., "Early voltage and saturation voltage improvement in deep sub-micron technologies using associations of transistors", SBCCI 08, September 1-4, 2008.

[15] Domeij, M. and Lee, H. S., "SiC power bipolar junction transistors modeling and improvement of the current gain", Power Electronics and Applications, pp. p-7.

[16] Kumar, M. J. and Parihar, V., "Surface accumulation layer transistor (SALTran): a new bipolar transistor for enhanced current gain and reduced hot-carrier degradation", IEEE Transactions on Device and Materials Reliability, vol. 4, no. 3, 2004.

[17] Domeij, M. and Lee, H. S., "High current gain silicon carbide bipolar power transistors", International Symposium on Power Semiconductor Devices and IC's, Naples, Italy, June 4-8, 2006.

[18] Suzuki, K., "Optimum base doping profile for minimum base transit time considering velocity saturation at base-collector junction and dependence of mobility and bandgap narrowing on doping concentration", IEEE Tran. on Electron Devices, vol. 48, pp. 2102-2107, 2001.

[19] Zareba, A., Łukasiak, L. and Jakubowski, A., "The Influence of selected material and transport parameters on the accuracy of modeling early voltage in SiGe-base HBT", IEEE Transactions on Electron Devices, vol. 53, no. 8, 2006.

[20] Babcock, J.A.; Li Jen Choi; Sadovnikov, A.; van Noort, W.; Estonilo, C.; Allard, P.; Ruby, S.; Cestra, G.;" Temperature interaction of Early voltage, current gain and breakdown characteristics of *n-p-n* and *pnp* SiGe HBTs on SOI" Bipolar/BiCMOS Circuits and Technology Meeting (BCTM), 2010.

[21] Babcock, J.A., Sadovnikov, A., Li J. C., van Noort, W.; Allard, P., Cestra, G.,'' Forward and inverse mode Early voltage dependence on current and temperature for advanced SiGe-pnp on SOI", Bipolar/BiCMOS Circuits and Technology Meeting (BCTM), 2011.

[22] Xiao-B. X., He-Ming Z., Hui-Yong H., Jiang T. Q., "Early effect of SiGe heterojunction bipolar transistors", School of Microelectronics, Xidian University, Xi'an Shaanxi 710071, PR China, Solid State Electronics 2012.

[23] Patri, V. S. and Kumar, M. J., "Profile design considerations for minimizing base transit time in SiGe HBT's", IEEE Tran. on Electron Devices, vol. 45, pp. 1725-1731, 1998.

[24] Hochheiser, S., "The transistor and portable electronics", IEEE Global History Network, 2008.

[25] Arns, R. G. "The other transistor: early history of the metal-oxide-semiconductor field-effect transistor", Engineering Science and Education Journal, vol. 7, pp. 233–240, 1998.

[26] Heywang, W. and Zaininger, K. H., "Silicon: the semiconductor material, evolution and future of a technology", Springer, 2004.

[27] Snowden, C. M. and Snowden, E., "Introduction to semiconductor device modelling", World Scientific Publishing Co, Singapore, 1998.

[28] Sze, S. M. and Ng, K. K., "Physics of semiconductor devices, 3rd edition", New Jersey: Jown Wiley & Sons, 2007.

[29] Levy, R. A., "Microelectronic materials and processes", Kluwer Academic Publisher, 1989.

[30] Streetman, B. G.," Solid state electronic devices, 4th edition", Prentice Hall, 1995.

[31] Grens, C. M., Cheng, P. and Cressler, J. D., "An investigation of the large-signal RF safe-operating-area on aggressively-biased cascode SiGe HBTs for power amplifier applications", Silicon Monolithic Integrated Circuits in RF System, pp. 1-4, 2009.

[32] Asbeck, P.," Handbook of thin film devices", vol. 1, Academic Press, 2000.

[33] "The Nobel prize in physics," URL http://nobelprize.org/nobel_prizes/2000.

[34] Cressler, J. D. and Niu, G., "Silicon-Germanium heterojunction bipolar transistors".

[35] Jain, S. C., "Germanium-Silicon strained layers and heterostructures", Academic Press, Inc. USA, 1994.

[36] Harame, D. L., Ahlgren, D. D., Coolbaugh, J. S., Dunn, G. G., Freeman, J. D., Gillis, R. A., Groves, G. N., Hendersen, R. A., Johnson, A. J., Joseph, S., Subbanna, A. M., Victor, K. M., Watson, C. S., Webtser and Zampardi, P. J., "Current status and future trends of SiGe BiCMOS technology", IEEE Trans. on Electron Devices, vol. 48, pp. 2575−2593, 2001.

[37] Zhang, G., Cressler, J. D., Niu, G. and Pinto, A., "A comparison of *n-p-n* and pnp profile design tradeoffs for complementary SiGe HBT technology", Solid-State Electronics, vol. 44, pp. 1949−1954, 2000.

[38] Lombardo, S., Raineri, V., Via, F. L., Iacona, F., Campisano, S. U., Pinto, A. and Ward, P., "Ge-ion implantation in silicon for the fabrication of silicon/SiGe heterojunction transistors", Material Chemistry and Physics, vol. 46, pp. 156−160, 1996.

[39] Hamel, J. S., Tang, Y. T. and Osman, K., "Technological requirements for a lateral SiGe HBT technology including theoretical performance predictions relative to vertical SiGe HBTs", IEEE Trans. on Electron Devices, vol. 49, pp. 449−456, 2002.

[40]   Ahlgren, D. C., Freeman, G., Subbanna, S., Groves, R., Greenberg, D., "A SiGe HBT BiCMOS technology for mixed-signal RF applications", Proceedings of the Bipolar/BiCMOS Circuits and Technology Meeting, pp. 195-197, 1997.

[41]   Joseph, A., Coolbaugh, D., Zierak, M., Wuthrich, R., Geiss, P., He, Z., "A 0.18um BiCMOS technology featuring 120/100 GHz (fT/fmax) and ASIC-compatible CMOS using copper interconnect", Proceedings of the Bipolar/BiCMOS Circuits Circuit Tech. Meeting, Minneapolis, pp. 143-146, 2001.

[42]   Heinemann, B., Rucker, H., Barth, R., Bauer, J., Bolze, D., Bugiel, E., Drews, J., Ehwald, K.-E., Grabolla, T., Haak, U., Hoppner, W., Knoll, D., Kruger, D., Kuck, B., Kurps, R., "Novel collector design for high-speed SiGe:C HBTs", IEEE International Electron Device Meeting Technical Digest, pp. 775-778, 2002.

[43]   Heinemann, B., Barth, R., Bolze, D., Drews, J., Formanek, P., Grabolla, T., Haak, U., "A low-parasitic collector construction for high-speed SiGe:C HBTs", IEEE International Electron Device Meeting Technical Digest, pp. 251-254, 2004.

[44]   Heinemann, B., Barth, R., Bolze, D., Drews, J., Formanek, P., Fursenko, O., Glante, M., Glowatzki, K., Gregor, A., Haak, U., Hoppner, W., Knoll, D. R., "A complementary BiCMOS technology with high speed n-p-n and pnp SiGe:C HBTs", IEEE International Electron Device Meeting Technical Digest, pp. 117-120, 2003.

[45]   Kuo, W. M. L., Lu, Y., Floyd, B., Haugerud, B., Sutton, A., Krithivasan, R., Cressler, J. D., Gaucher, B., Marshall, P., Reed, R., Rieh, J.-S. and Freeman, G., "Total dose tolerance of monolithic millimeter-wave transceiver building blocks in 200 GHz SiGe technology," IEEE Trans. on Nuclear Science, vol. 51, pp. 3781-3787, 2004.

[46]   Nellis K. and Zampardi, P. "A comparison of linear handset power amplifiers in different bipolar technologies", IEEE Journal of Solid-State Circuits, vol. 39, pp. 1746-1754, 2004.

[47]   Zerounian, N., Aniel, F., Barbalat, B., Chevalier, P. and Chantre, A., "500 GHz cutoff frequency SiGe HBTs", Electronics Letters, vol. 43, pp. 774–775, 2007.

[48]   Hughes, B., "A temperature noise model for extrinsic FET's", IEEE Trans. on Microwave Theory and Techniques, vol. 40, pp. 1821-1832, 1992.

[49]   Larson, L., "Integrated circuit technology options for RFIC's -present status and future directions," IEEE Journal of Solid-State Circuits, vol. 33, pp. 387-399, 1998.

[50]   Mattisson, S., "Architecture and technology for multistandard transceivers", Proceedings of the Bipolar/BiCMOS Circuits and Technology Meeting (BCTM), pp. 82-85, September 2001.

[51] Lie, D. Y. C., Yota, J., Xia, W., Joshi, A. B., Williams, R. A., Zwingman, R., Chung, L. and Kwong, D. L., "New experimental findings on process-induced hot-carrier degradation of deep-submicron N-MOSFETs", IEEE International Reliability Physics Symposium, pp. 362-369, 1999.

[52] Lie, D. Y. C., Yuan, X., Larson, L. E., Wang, Y. H., Senior, A. and Mecke, J., "RF-SoC: low-power single-chip radio design using Si/SiGe BiCMOS technology," Proceedings of the 3rd International Microwave and MillimeterWave Technology, pp. 30-37, 2002.

[53] Yuan, X., Lie, D. Y. C., Larson, L. E., Blonski, J., Gross, J., Kumar, M., Mecke, J., Senior, A., Chen, Y., Pho, A. and Harame, D., "RF linearity study of SiGe HBTs for low power RFIC design I", Proceedings of the 3rd International Microwave and Millimeter Wave Technology, pp. 70-73, 2002.

[54] Niu, Z. Xu, G., Luo, L., Chakraborty, P. S., Cheng, P., Thomas, D. and Cressler, J. D., "Cryogenic RF small-signal modeling and parameter extraction of SiGe HBTs," IEEE Topical Meeting on Silicon Monolithic Integrated Circuits in RF Systems, SiRF'09, pp. 1-4, 2009.

[55] Overstraeten, R. J. V., Deman, H. J. and Mertens, R. P., "Transport equation in heavy doped silicon", IEEE Trans. Electron Devices, vol. ED-20, pp. 290-298, 1973.

[56] Suzuki, K., "Optimum base doping profile for minimum base transit time", IEEE Truns. Electron Devices, vol. 38, pp. 2128-2133, 1991.

[57] Roulston, D. J., "Early voltage in very-narrow-base bipolar transistors", IEEE Electron Device Letter, vol. 11, pp. 88-89, 1990.

[58] Hassan, M. M. S. and Nomani, M. W. K., "Base transit time model considering field dependent mobility for BJTs operating at high-level injection", IEEE Trans. on Electron Devices, vol. 53, pp. 2532-2539, 2006.

[59] Tang, Z. R., Kamins, T. and Salama, C. A. T., "Analytical and experimental characteristics of SiGe HBT with thin α-Si : H emitters", Solid-State Electronics, vol. 38, pp. 1829-1834, 1995.

[60] Kwok K. H. and Selvakumar, C. R., "Profile design considerations for minimizing base transit time in SiGe HBTs for all levels of Injection before onset of Kirk effect", IEEE Trans. on Electron Devices, vol. 48, pp. 1540-1549, 2001.

[61] Yuan, J. S., "Effect of base profile on the base transit time of the bipolar transistor for all levels of injection", IEEE Trans. on Electron Devices, vol. 41, pp. 212-216, Feb 1994.

[62] Alamo, J. d., Swirhum, S. and Swanson, R. M., "Simultaneous measurement of hole lifetime, hole mobility and bandgap narrowing in heavily doped n-type silicon," IEDM Tech. Dig., pp. 290-293, 1985.

[63] Zareba, A., Lukasiak, L. and Jakubowski, A., "Modeling of SiGe-base heterojunction bipolar transistor with Gaussian doping distribution", Solid-State Electronics, vol. 45, pp. 2029-2032, 2001.

[64] Neamen, D. A., "Semiconductor physics and devices: basic principles, 3rd edition" New York: McGraw-Hill, 2003.

[65] Basu, S. "Analytical modeling of base transit time of SiGe HBTs including effect of temperature", International Semiconductor Conference, CAS'08, vol. 2, pp. 339-342, 2008.

[66] Chang, S. T., Liu, C. W. and Lu, S. C., "Base transit time of graded-base Si/SiGe HBTs considering recombination lifetime and velocity saturation", Solid-State Electronics, vol. 48, pp. 207–215, 2004.

[67] Chen, B. Y. and Kuo, J. B., "An accurate knee current model considering quasi-saturation for BJTs operating at high current density," Solid-State Electronics, vol. 38, pp. 1282–1284, 1995.

[68] Slotboom, J. W. and Graaf, H. C. D., "Measurement of bandgap narrowing in Si bipolar transistors," Solid-State Electronics, vol. 19, pp. 857–862, 1976.

[69] Lu, T. C. and Kuo, J. B. "A closed form analytical BJT forward transit time model considering bandgap narrowing effects and concentration dependent diffusion coefficients", Solid-State Electronics, vol. 35, pp. 1374–1377, 1993.

[70] Kroemer, H. "Two integral relations pertaining to electron transport through a bipolar transistor with a nonuniform energy gap in the base region", Solid-State Electronics, vol. 28, pp. 1101–1103, 1985.

[71] Suzuki, K. and Nakayama, N., "Base transit time of shallow-base bipolar transistors considering velocity saturation at base–collector junction", IEEE Trans. Electron Devices, vol. 39, pp. 623–628, 1993.

[72] Poon, H. C., Gummel, H. K. and Scharfetter, D. L., "High injection in epitaxial transistors", IEEE Trans. Electron Device, ED-16, 1969.

[73] Daw, A. N., Mitra, R. N. and Choudhury, N. K. D., "Cutoff frequency of a drift transistor", Solid State Electron, vol. 10, pp. 359-360, 1967.

[74] Hsieh, M.W., Ho, C.C., Wang, H.P., Lee, C.Y., Chen, G.J., Tang, D.T. and Chan, Y.J., "Frequency response improvement of 120 GHz f_T SiGe HBT by optimizing the contact configurations", Taiwan Semiconductor Manufacturing Company, pp 1-4.

[75] Prinz, E. J. and Sturm, J. C.,"Current gain-Early voltage products in heterojunction bipolar transistors with nonuniform base bandgaps", IEEE Electron Device Letters, vol. 12, no. 12, December 1991.

[76]   Freeman, G., Meghelli, M., Kwark, Y., Zier, S., Rylyakov, A., Sorna, M.A., Tanji, T. O., Schreiber, K., Walter, J. S., Rieh, B., Jagannathan, A., Joseph and Subbanna, S., "40 Gb/s circuits built from a 120 GHz f_T SiGe technology", IEEE J. Solid State Circuits, vol. 37 no. 9, pp. 1106-1114, 2002.